Electronic Supplementary Material (ESI) for Dalton Transactions.

Ruthenium-arene complexes bearing naphthyl-substituted 1,3-dioxoindan-2-carboxamides ligands for G-quadruplex DNA recognition

Laura A. Hager,[1] Stephan Mokesch,[1] Claudia Kieler,[2] Silvia Alonso-de Castro,[3] Dina Baier,[2] Alexander Roller,[1] Wolfgang Kandioller,[1] Bernhard K. Keppler,[1] Walter Berger,[2] Luca Salassa,[3,4] Alessio Terenzi*[1,2]

[1] Institute of Inorganic Chemistry, Faculty of Chemistry University of Vienna, Waehringerstrasse 42, A-1090 Vienna, Austria.

[2] Department of Medicine I, Institute of Cancer Research and Comprehensive Cancer Center, Medical University Vienna, Borschkegasse 8a, A-1090 Vienna, Austria.

[3] Donostia International Physics Center, Paseo Manuel de Lardizabal 4, Donostia, 20018, Spain

[4] Ikerbasque, Basque Foundation for Science, Bilbao, 48013, Spain

*E-mail: aterenzi@dipc.org

Supporting Information

Table S1. Experimental parameter and CCDC-Code.

Sample	Machine	Source	Temp.	Detector Distance	Time/ Frame	#Frames	Frame width	CCDC
	Bruker		[K]	[mm]	[s]		[°]	
1a	X8	Mo	100	35	3	995	0.5	1870492
1b	X8	Mo	100	35	10	534	0.5	1870493
2a	D8	Mo	100	34	10	664	0.5	1870494

Table S2. Sample and crystal data of **1a**.

Chemical formula	$C_{31}H_{28}ClNO_3Ru$	**Crystal system**	monoclinic	
Formula weight [g/mol]	599.06	**Space group**	*P2/n*	
Temperature [K]	100	**Z**	8	
Measurement method	\f and \w scans	**Volume [Å^3]**	5251.8(3)	
Radiation (Wavelength [Å])	MoKα (λ = 0.71073)	**Unit cell dimensions [Å] and [°]**	22.1184(8)	90
Crystal size / [mm^3]	0.24 × 0.2 × 0.07		10.0442(3)	105.602(2)
Crystal habit	clear orange block		24.5438(9)	90
Density (calculated) / [g/cm^3]	1515	**Absorption coefficient / [mm^{-1}]**	0.733	
Abs. correction Tmin	0.6831	**Abs. correction Tmax**	0.7460	
Abs. correction type	multiscan	**F(000) [e$^-$]**	2448.0	

Table S3. Data collection and structure refinement of **1a**.

Index ranges	-30 ≤ h ≤ 31, -14 ≤ k ≤ 14, -34 ≤ l ≤ 34	**Theta range for data collection [°]**	4.406 to 60.17	
Reflections number	71690	**Data / restraints / parameters**	15423/0/673	
Refinement method	Least squares	**Final R indices**	all data	R1 = 0.0519, wR2 = 0.0810
Function minimized	$\Sigma w(F_o^2 - F_c^2)^2$		I>2σ(I)	R1 = 0.0344, wR2 = 0.0733
Goodness-of-fit on F^2	1061	**Weighting scheme**	$w=1/[\sigma^2(F_o^2)+(0.0308P)^2+1.5017P]$	
Largest diff. peak and hole [e Å^{-3}]	0.64/-0.89		where $P=(F_o^2+2F_c^2)/3$	

Table S4. Sample and crystal data of **1b**.

Chemical formula	$C_{36}H_{33}F_6N_2O_3PRu$	**Crystal system**	monoclinic	
Formula weight [g/mol]	787.68	**Space group**	*P21/n*	
Temperature [K]	100.0	**Z**	4	
Measurement method	\f and \w scans	**Volume [Å^3]**	3302.5(4)	
Radiation (Wavelength [Å])	MoKα (λ = 0.71073)	**Unit cell dimensions [Å] and [°]**	13.8315(10)	90
Crystal size / [mm^3]	0.1 × 0.1 × 0.05		15.1456(7)	109.345(2)
Crystal habit	clear yellow block		16.7083(11)	90
Density (calculated) / [g/cm^3]	1584	**Absorption coefficient / [mm^{-1}]**	0.597	
Abs. correction Tmin	0.6831	**Abs. correction Tmax**	0.7460	
Abs. correction type	multiscan	**F(000) [e$^-$]**	1600.0	

Table S5. Data collection and structure refinement of **1b**.

Index ranges	-14 ≤ h ≤ 16, -15 ≤ k ≤ 18, -19 ≤ l ≤ 20	**Theta range for data collection [°]**	4.278 to 50.792	
Reflections number	18959	**Data / restraints / parameters**	6056/0/445	
Refinement method	Least squares	**Final R indices**	all data	R1 = 0.0759, wR2 = 0.1240
Function minimized	$\Sigma w(F_o^2 - F_c^2)^2$		I>2σ(I)	R1 = 0.0474, wR2 = 0.1083
Goodness-of-fit on F^2	1053	**Weighting scheme**	$w=1/[\sigma^2(F_o^2)+(0.0566P)^2+1.0082P]$	
Largest diff. peak and hole [e Å^{-3}]	0.78/-0.61		where $P=(F_o^2+2F_c^2)/3$	

Table S1. Sample and crystal data of **2a**.

Chemical formula	$C_{32}H_{31.33}ClNO_{3.67}Ru$	**Crystal system**	monoclinic	
Formula weight [g/mol]	625.11	**Space group**	*Cc*	
Temperature [K]	100.0	**Z**	4	
Measurement method	\f and \w scans	**Volume [Å^3]**	2795.46(18)	
Radiation (Wavelength [Å])	MoKα (λ = 0.71073)	**Unit cell dimensions [Å] and [°]**	20.9813(8)	90
Crystal size / [mm^3]	0.274 × 0.231 × 0.119		10.3997(4)	117.7999(10)
Crystal habit	clear orange block		14.4831(5)	90
Density (calculated) / [g/cm^3]	1485	**Absorption coefficient / [mm^{-1}]**	0.693	
Abs. correction Tmin	0.6496	**Abs. correction Tmax**	0.7460	
Abs. correction type	multiscan	**F(000) [e$^-$]**	1283.0	

Table S2. Data collection and structure refinement of **2a**.

Index ranges	-25 ≤ h ≤ 25, -12 ≤ k ≤ 12, -17 ≤ l ≤ 17	**Theta range for data collection [°]**	7.664 to 50.7	
Reflections number	11956	**Data / restraints / parameters**	4966/2/364	
Refinement method	Least squares	**Final R indices**	all data	R1 = 0.0157, wR2 = 0.0390
Function minimized	$\Sigma w(F_o^2 - F_c^2)^2$		I>2σ(I)	R1 = 0.0155, wR2 = 0.0389
Goodness-of-fit on F^2	1065	**Weighting scheme**	$w=1/[\sigma^2(F_o^2)+(0.0084P)^2+1.8890P]$	
Largest diff. peak and hole [e $Å^{-3}$]	0.22/-0.46		where $P=(F_o^2+2F_c^2)/3$	

Table S8. 5'-3' sequences of the oligonucleotides used. The FRET probes used were FAM (6-carboxyfluorescein) and TAMRA (6-carboxy-tetramethylrhodamine). As model for ds-DNA the TATAGCTA-Heg-TATAGCTATA sequence was used (Heg linker = $[(-CH_2-CH_2-O-)_6]$).

Oligos	Sequence
dsDNA	TATAGCTATA-Heg-TATAGCTATA
hTelo	AGG GTT AGG GTT AGG GTT AGG G
c-Kit1	AGG GAG GGC GCT GGG AGG AGG G
bcl2	AGG GGC GGG CGC GGG AGG AAG GGG GCG GGA GCG GGG CTG
hTERT	GGG GGC TGG GCC GGG GAC CCG GGA GGG GTC GGG ACG GGG CGG GG

Table S9. $\Delta T_{1/2}$ values of 0.2 μM ds-DNA and G4s upon interaction with 4 μM binders. Uncertainty is ≤ 0.5 for the $\Delta T_{1/2}$ reported. Incubation time: 1h (compared with the values of 2h incubation time).

	ΔT (°C)				
	dsDNA	***hTelo***	***c-Kit1***	***Bcl2***	***hTERT***
1a (1h)	4.1	4.9	14.6	4.0	1.1
1a (2h)	4.0	0.9	-0.1	1.2	2.7
2a (1h)	3.4	16.0	19.6	8.3	13.1
2a (2h)	10.4	3.0	1.8	3.7	2.6
1b (1h)	3.4	16.0	24.0	8.3	13.1
1b (2h)	10.2	11.0	20.9	5.1	9.5
2b (1h)	6.1	21.8	23.9	10.4	11.5
2b (2h)	9.7	6.5	15.7	3.8	9.4

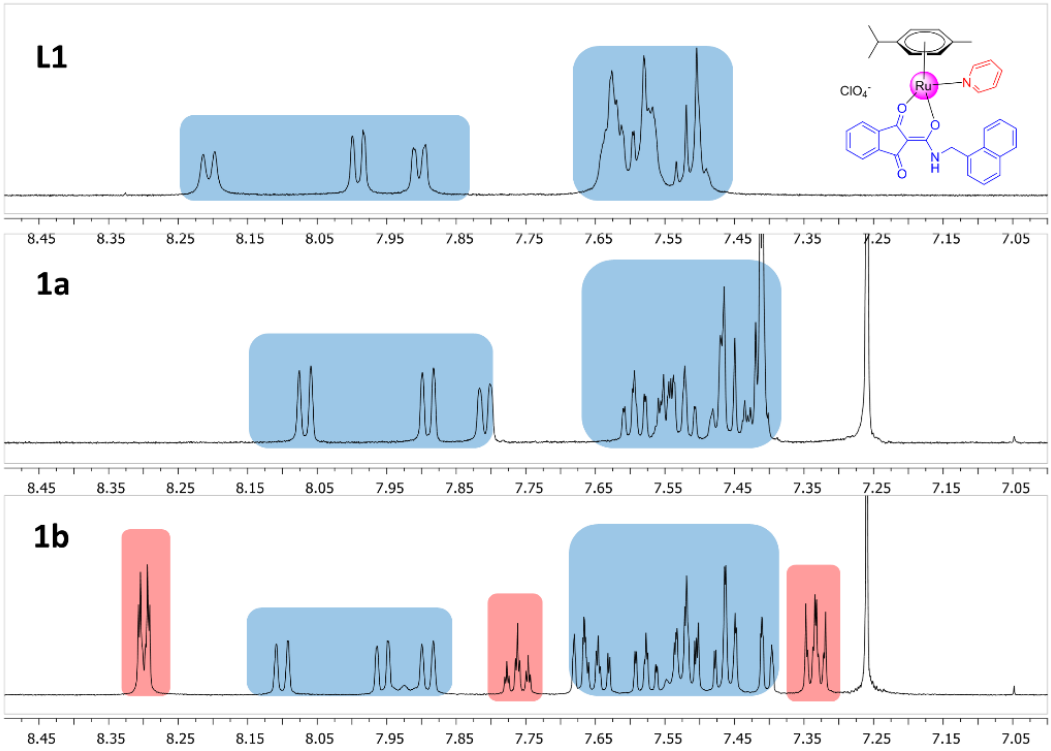

Figure S1. ^{1}H-NMR spectra of **L1** in deuterated DMSO and **1a-b** in $CDCl_3$. In red are highlighted the peaks corresponding to the pyridine protons.

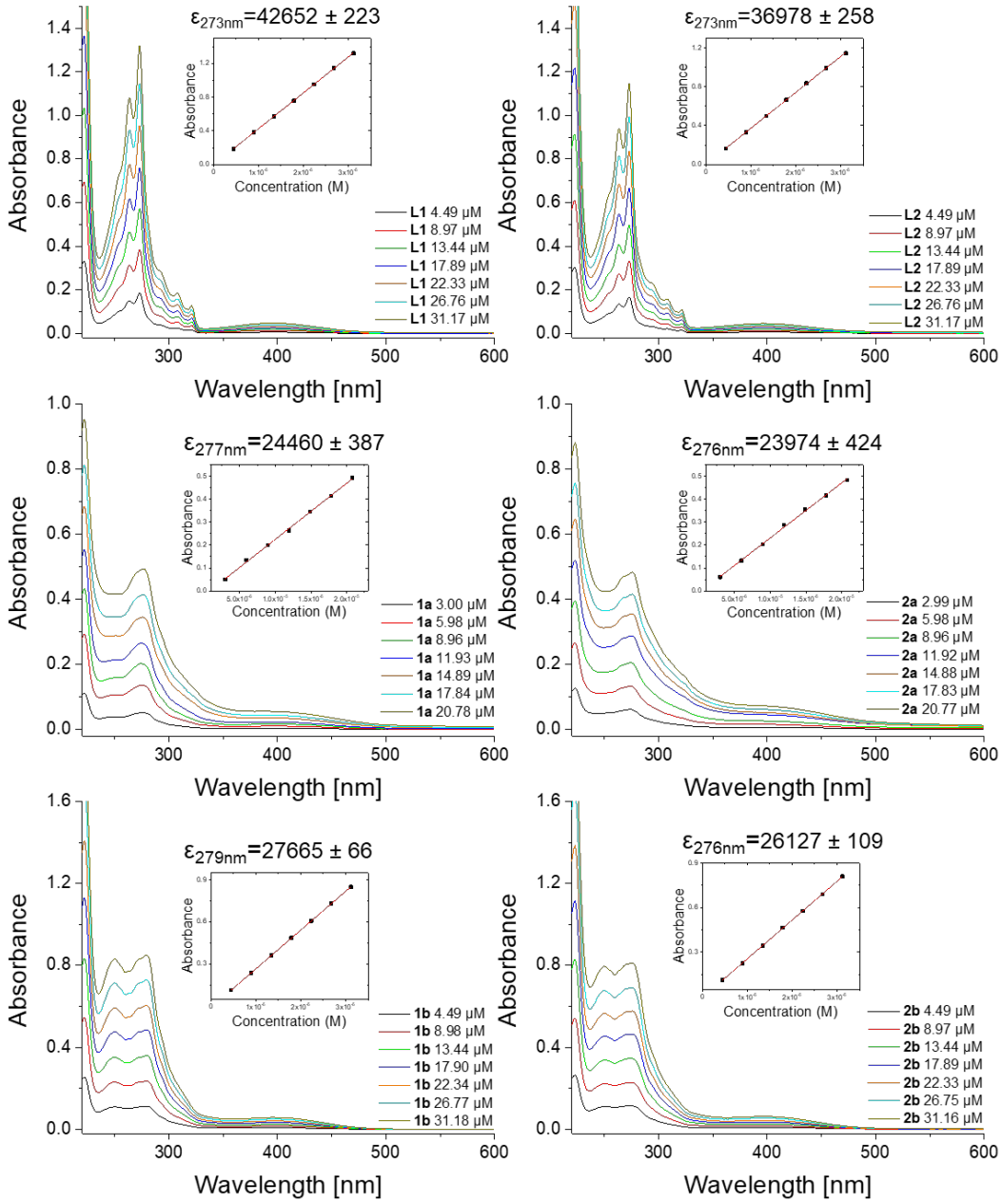

Figure S2. Spectra at 25 °C of the synthetized compounds at different concentrations. Linear regressions and the corresponding extinction coefficient (ε) are reported in the insets. Buffer: MES 2 mM, pH=6.0.

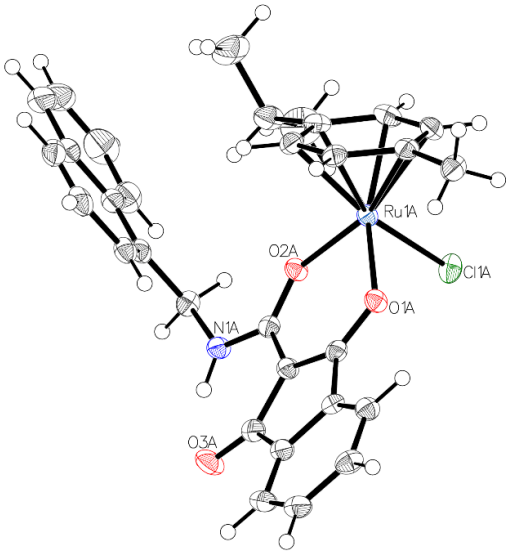

Figure S3. Crystal structure of **1a**. Anisotropic displacement ellipsoids visualized with 50% probability. Second independent molecule of the asymmetric unit omitted for clarity. Bond precision: C-C = 0.0032 Å.

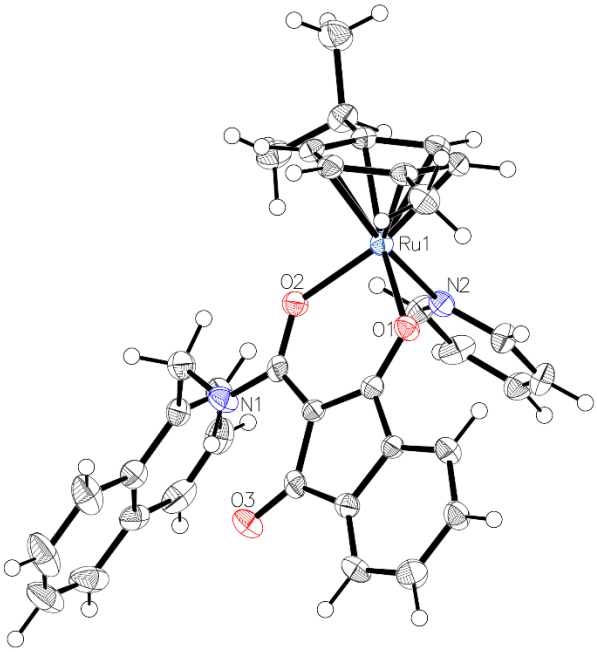

Figure S4. Crystal structure of **1b**. Anisotropic displacement ellipsoids visualized with 50% probability. Counter Ion omitted for clarity. Bond precision: C-C = 0.0069 Å.

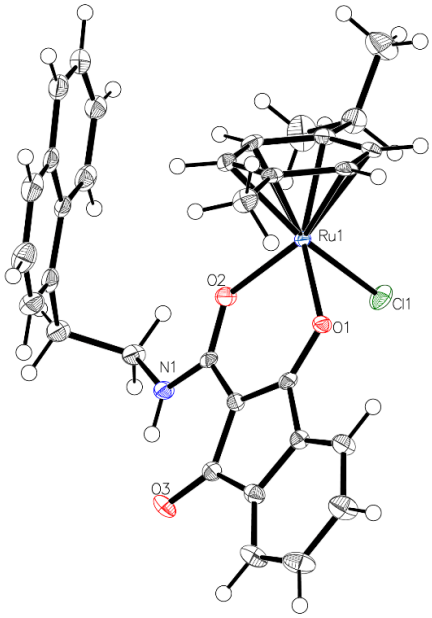

Figure S5. Crystal structure of **2a**. Anisotropic displacement ellipsoids visualized with 50% probability. Disordered solvent omitted for clarity. Bond precision: C-C = 0.0047 Å.

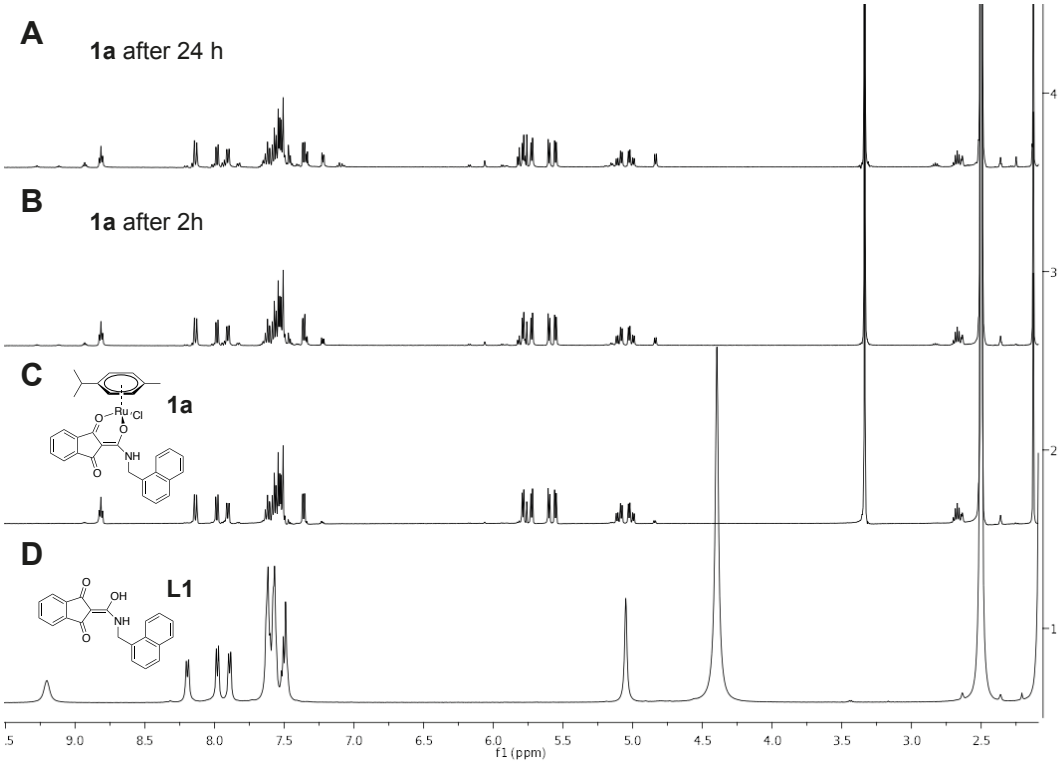

Figure S6. Stability of **1a** in DMSO: **A-C** ^{1}H-NMR spectra of compound **1a** in d_6-DMSO after 24 h, 2 h, and immediately after dissolving the compound. **D** ^{1}H-NMR spectrum of the ligand **L1** for comparison. Ligand **L1** is clearly not released after 24h, while only minor changes are observable (e.g. peak at 4.85 ppm) probably due to chloride ligand exchange.

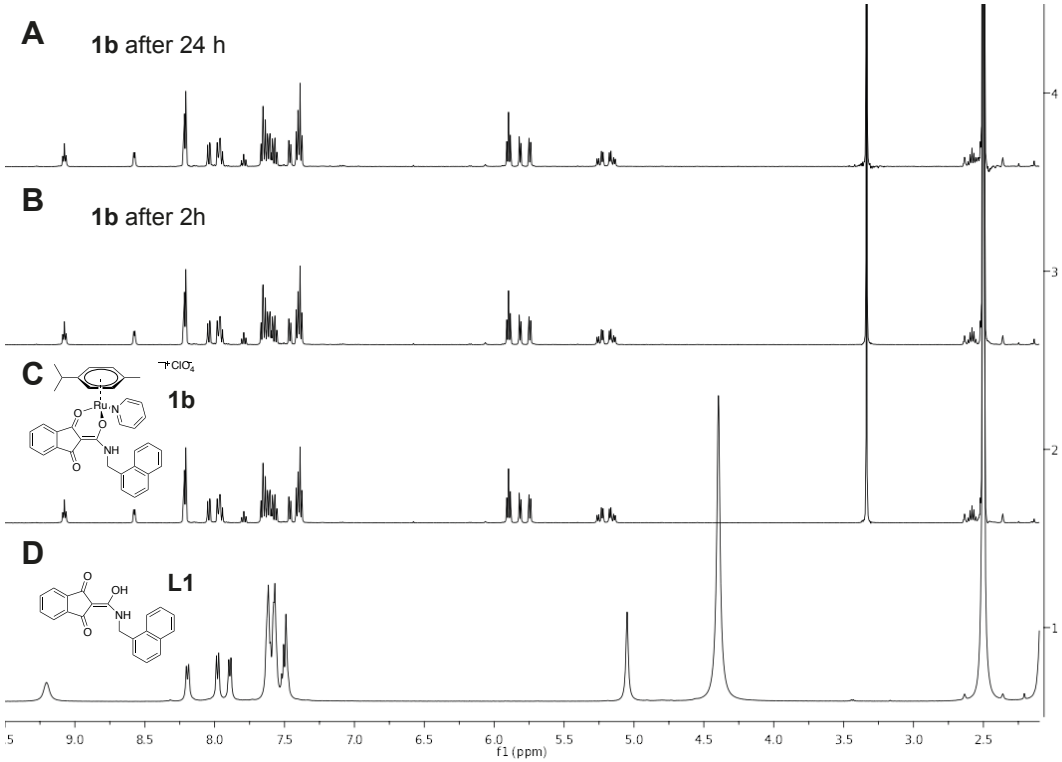

Figure S7. Stability of **1b** in DMSO: **A-C** ^{1}H-NMR spectra of compound **1b** in d_6-DMSO after 24 h, 2 h, and immediately after dissolving the compound. **D** ^{1}H-NMR spectrum of the ligand **L1** for comparison. Ligand **L1** is clearly not released after 24h.

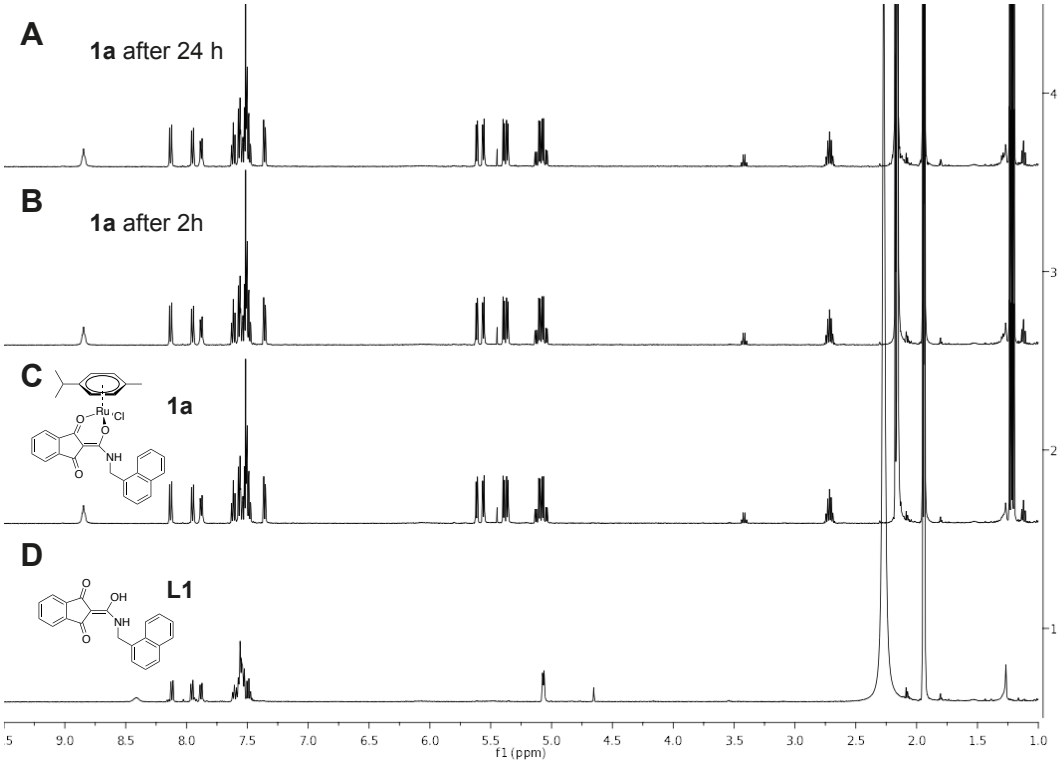

Figure S8. Stability of **1a** in acetonitrile: **A-C** ^{1}H-NMR spectra of compound **1a** in d_3-acetonitrile after 24 h, 2 h, and immediately after dissolving the compound. **D** ^{1}H-NMR spectrum of the ligand **L1** for comparison. Ligand **L1** is clearly not released after 24h.

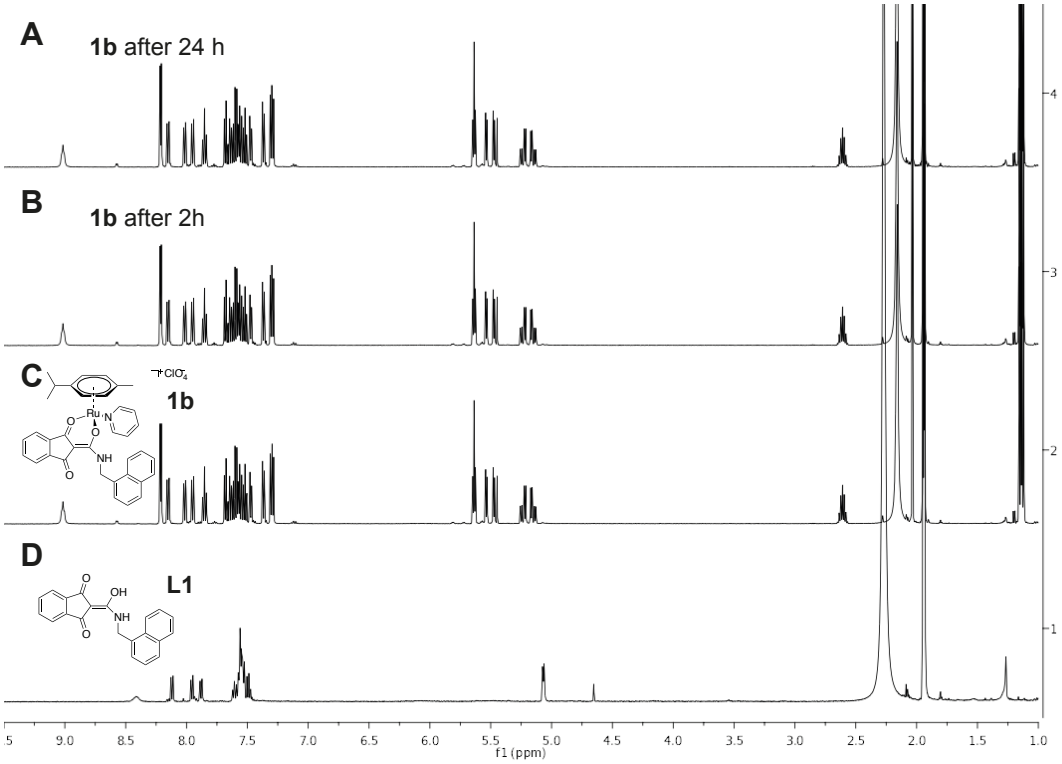

Figure S9. Stability of **1b** in acetonitrile: **A-C** ^{1}H-NMR spectra of compound **1b** in d_3-acetonitrile after 24 h, 2 h, and immediately after dissolving the compound. **D** ^{1}H-NMR spectrum of the ligand **L1** for comparison. . Ligand **L1** is clearly not released after 24h.

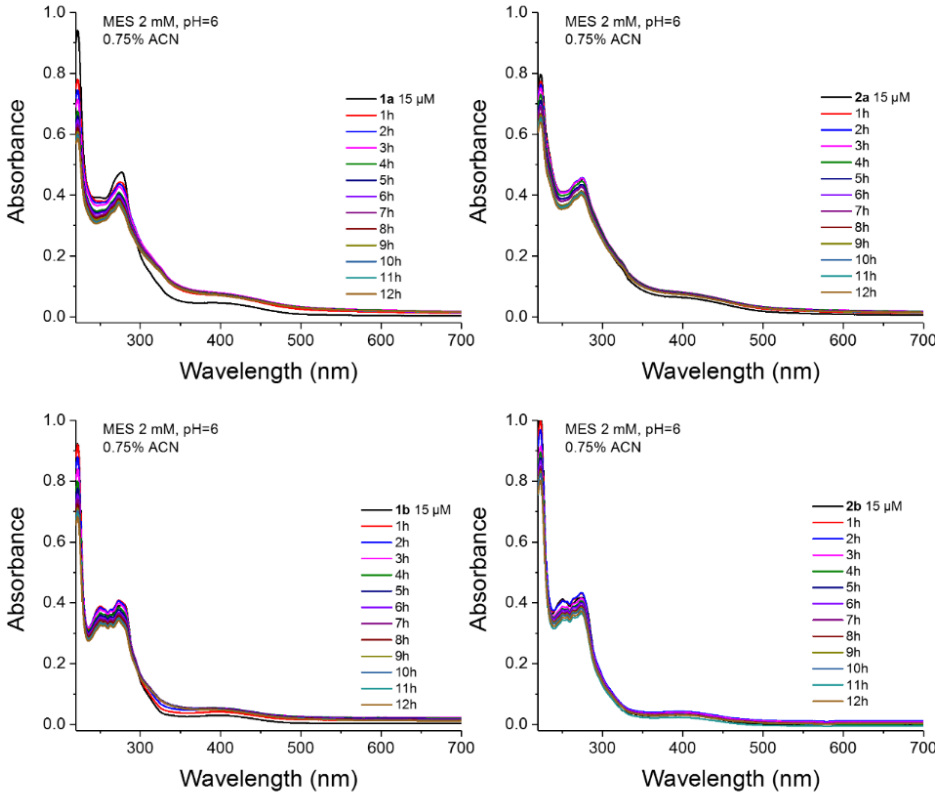

Figure S10. Time dependent UV-Vis spectra at 25 °C of compounds **1a-b** and **2a-b** at the indicated concentrations. Buffer: MES 2 mM, pH=6.0. UV-Vis spectra show no significant changes on FRET relevant time scales (incubation time 1-2 h), indicating their stability in these conditions, even if a slight tendency to precipitate over time have been observed.

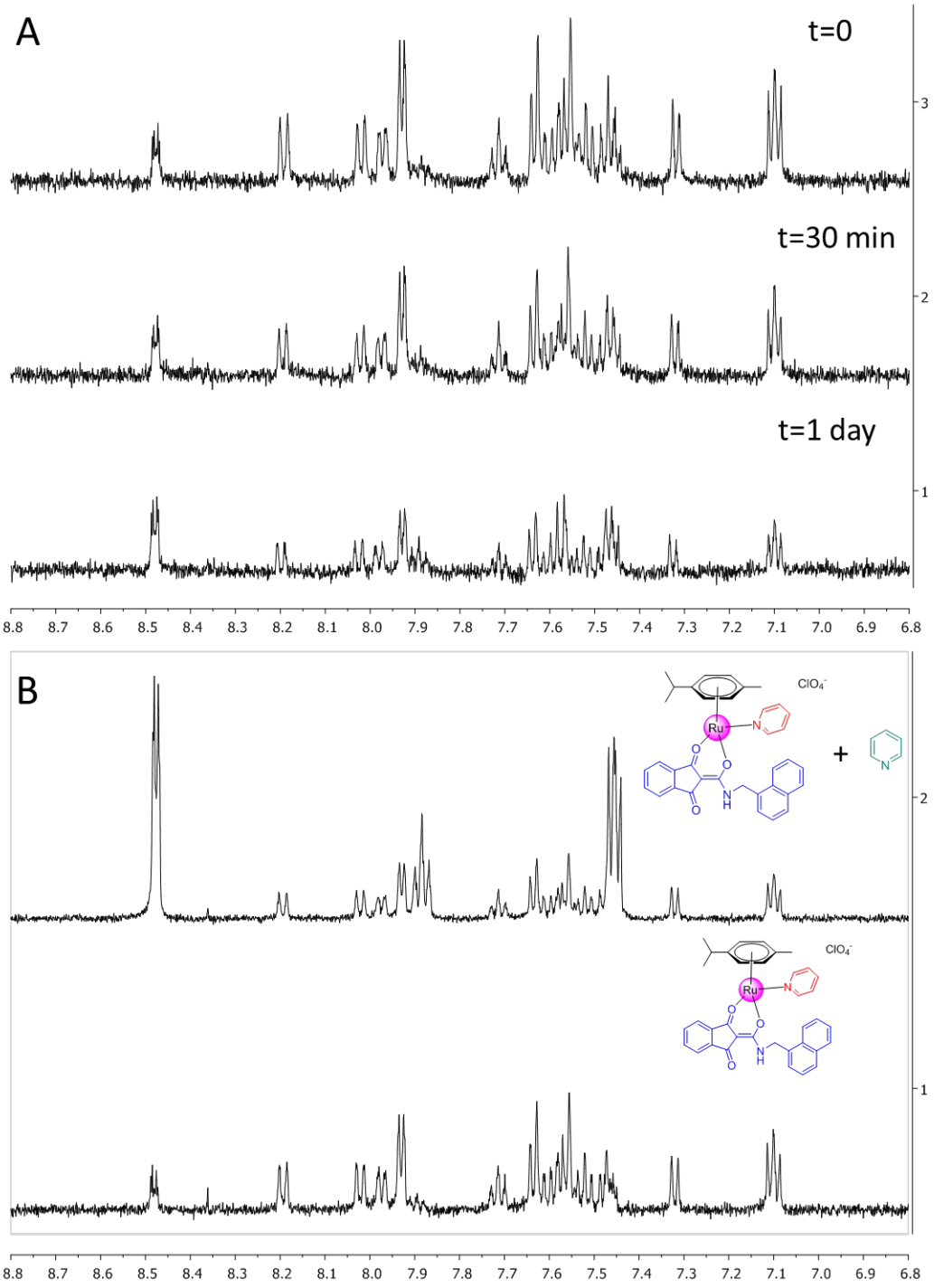

Figure S11. (A) Time-dependent ^{1}H-NMR spectra of **1b** in 2 mM MES buffer (10% D_2O, 8% DMSO-d6), pH=6. **1b** NMR spectrum does not change significantly after 1 day. (B) ^{1}H-NMR spectra of **1b** in 2 mM MES buffer (10% D_2O, 8% DMSO-d6) in the presence and absence of pyridine. No cleavage of the N-donor ligand was observed as can be demonstrated by addition of free pyridine. The peaks of the coordinated and free pyridine protons can be clearly distinguished.

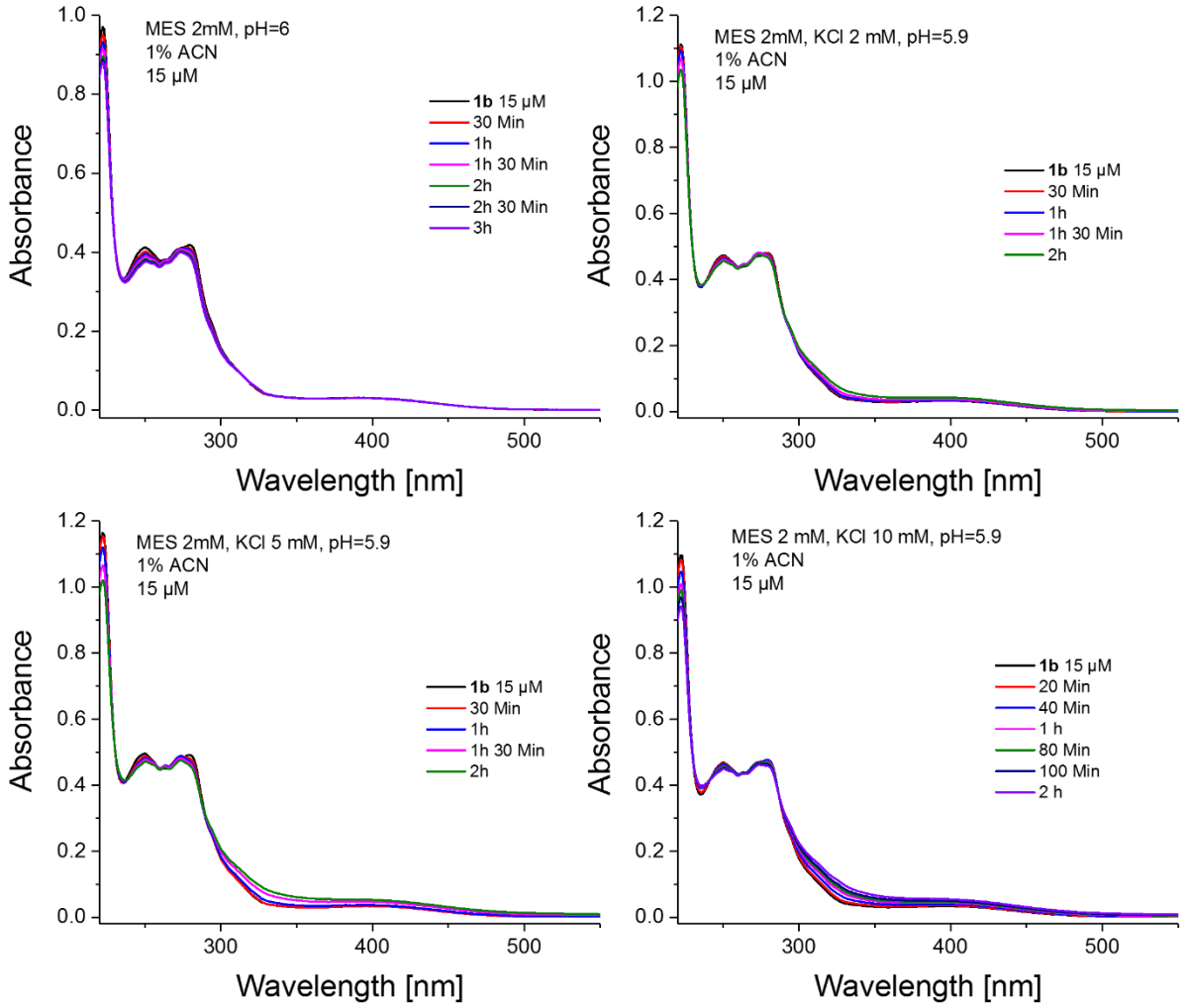

Figure S12. Time-dependent UV-Vis spectra at 25 °C of 15 µM **1b** in 2 mM MES buffer (pH=6.0) in the absence and in the presence of increasing concentration of KCl. Compound **1b**, selected as example of pyridine containing compound, is relatively stable increasing the concentration of KCl.

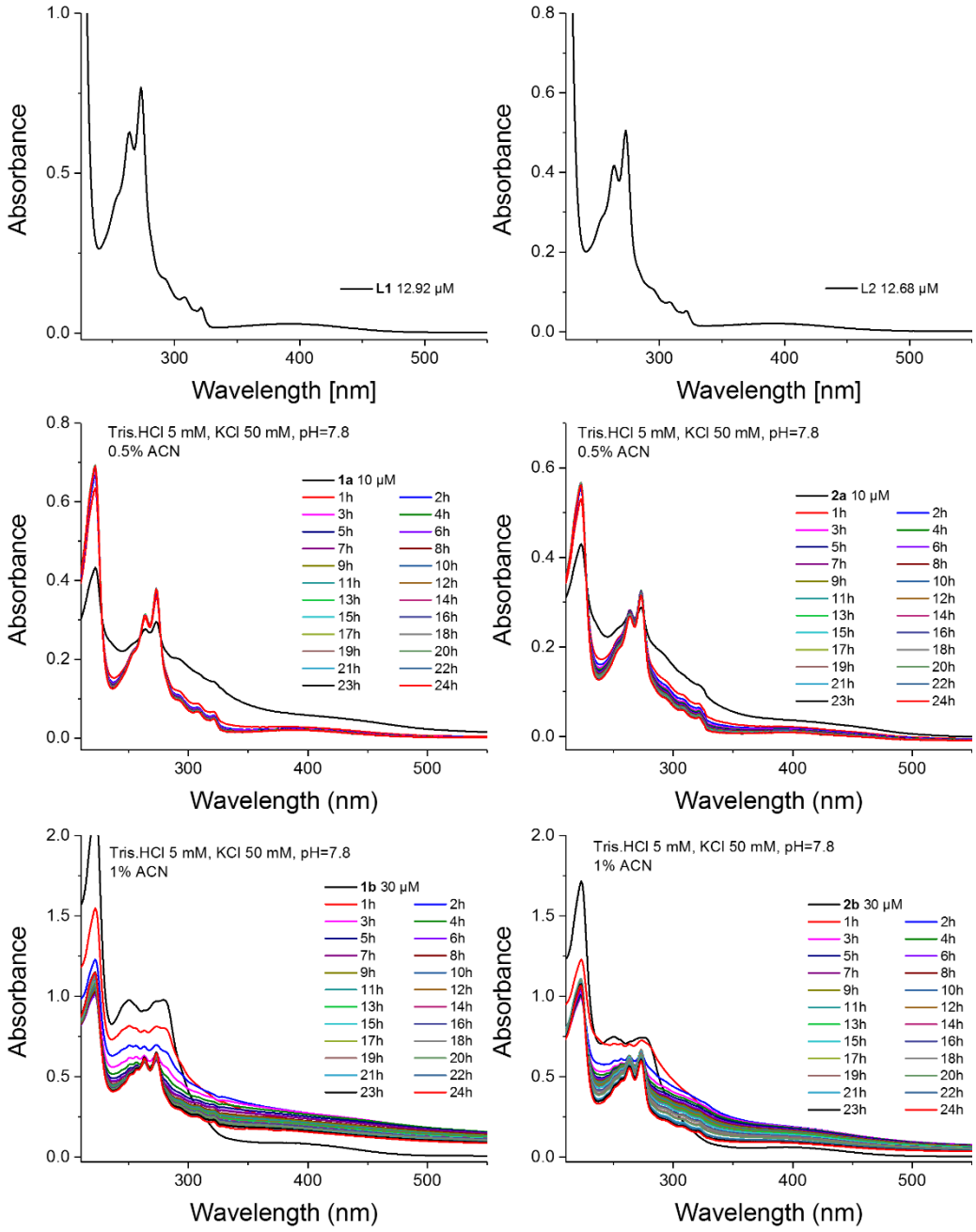

Figure S13. UV-Vis spectra at 25 °C in Tris-HCl 5 mM, KCl 50 mM, pH=7.8, of the ligands **L1** and **L2** and time-dependent spectra UV-Vis of compounds **1a-b** and **2a-b** at the indicated concentrations. The chlorido complexes **1a** and **2a** are quite unstable with the release of the1,3-dioxoindan-2-carboxamide ligand after only 1h as shown by the appearance of typical intense two-peaks band centered at 273 and 264 nm after 1h. The pyridine derivatives **1b** and **2b** are more stable on FRET relevant time scales (incubation time 1-2 h) but eventually, after 4h, also give rise to the release of the chelating ligand.

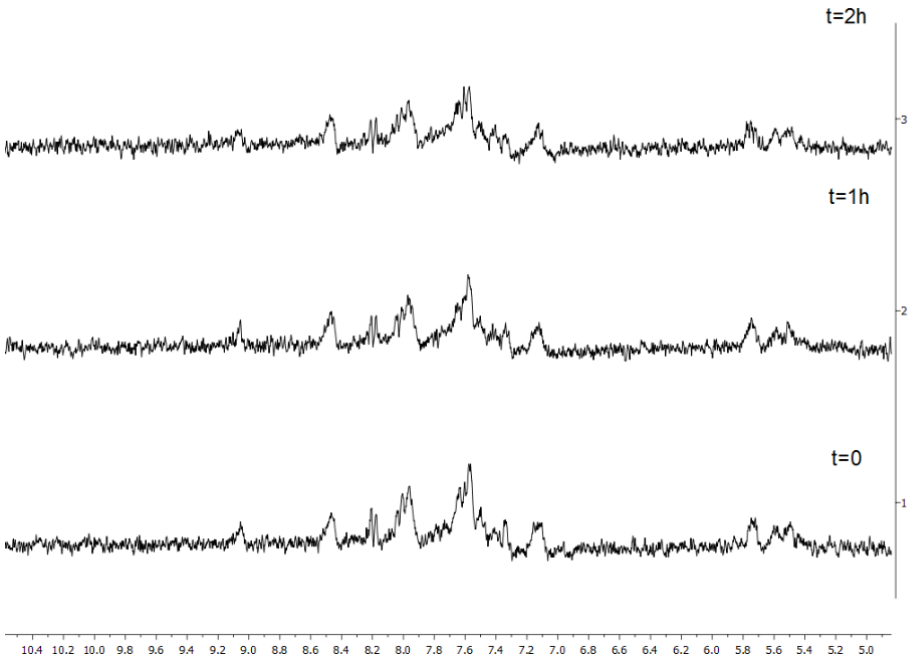

Figure S14. Time-dependent ^{1}H-NMR spectra of 150 μM **1b** in 60 mM cacodylate buffer (10% D_2O, 8% DMSO-d6), pH=7.2. **1b** NMR spectrum does not change after 2h, which is the limit incubation time in the FRET experiments.

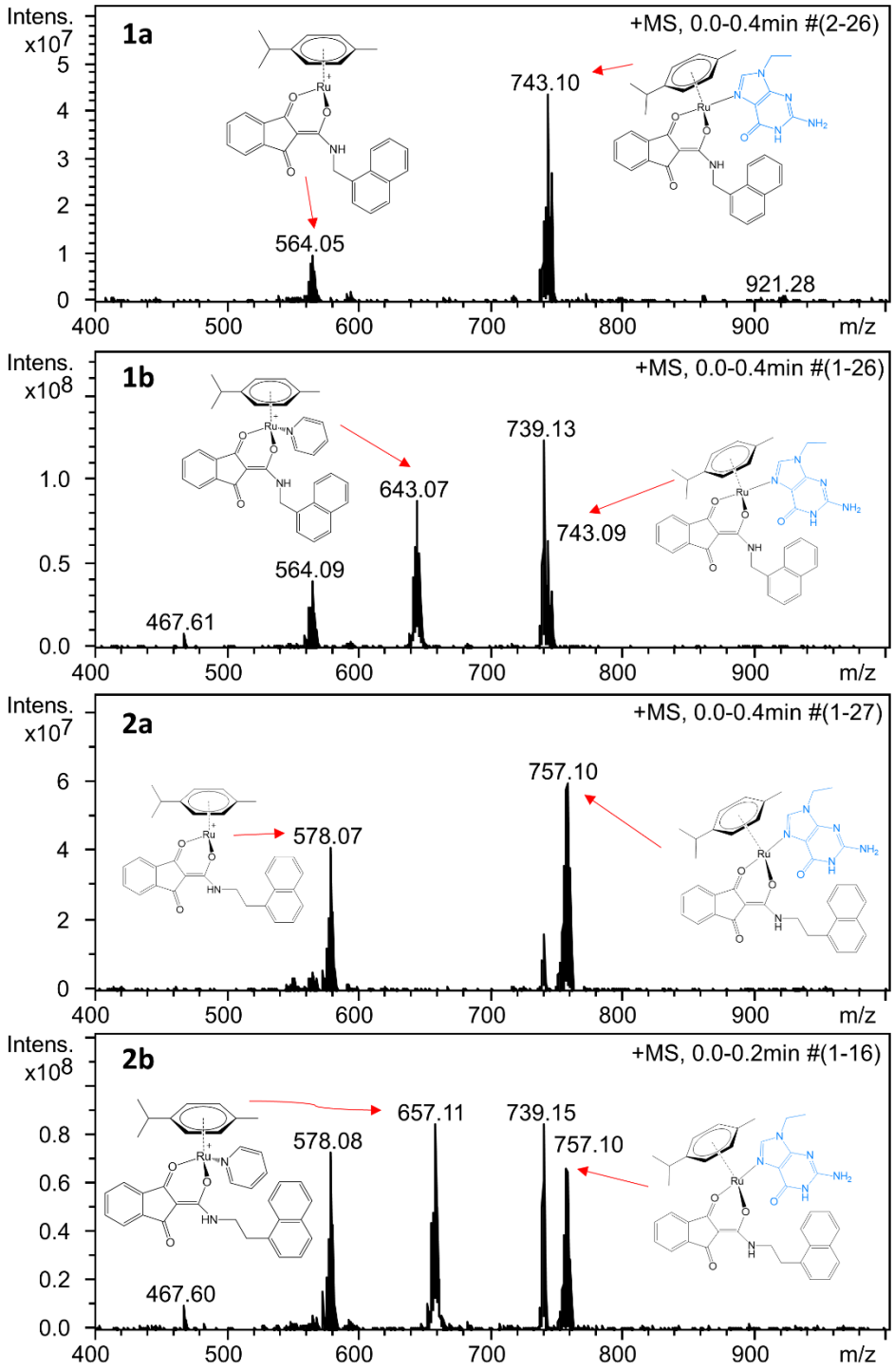

Figure S15. Mass spectra of 9-ethylguanine incubated (2 h) with the ruthenium complexes **1a-b** and **2a-b** (H_2O with 20% MeOH). Final concentrations in MeOH/H_2O before injection were 0.2 mM for the metal compounds and 0.6 mM for 9-EtG. All the compounds coordinated 9-EtG forming stable adducts.

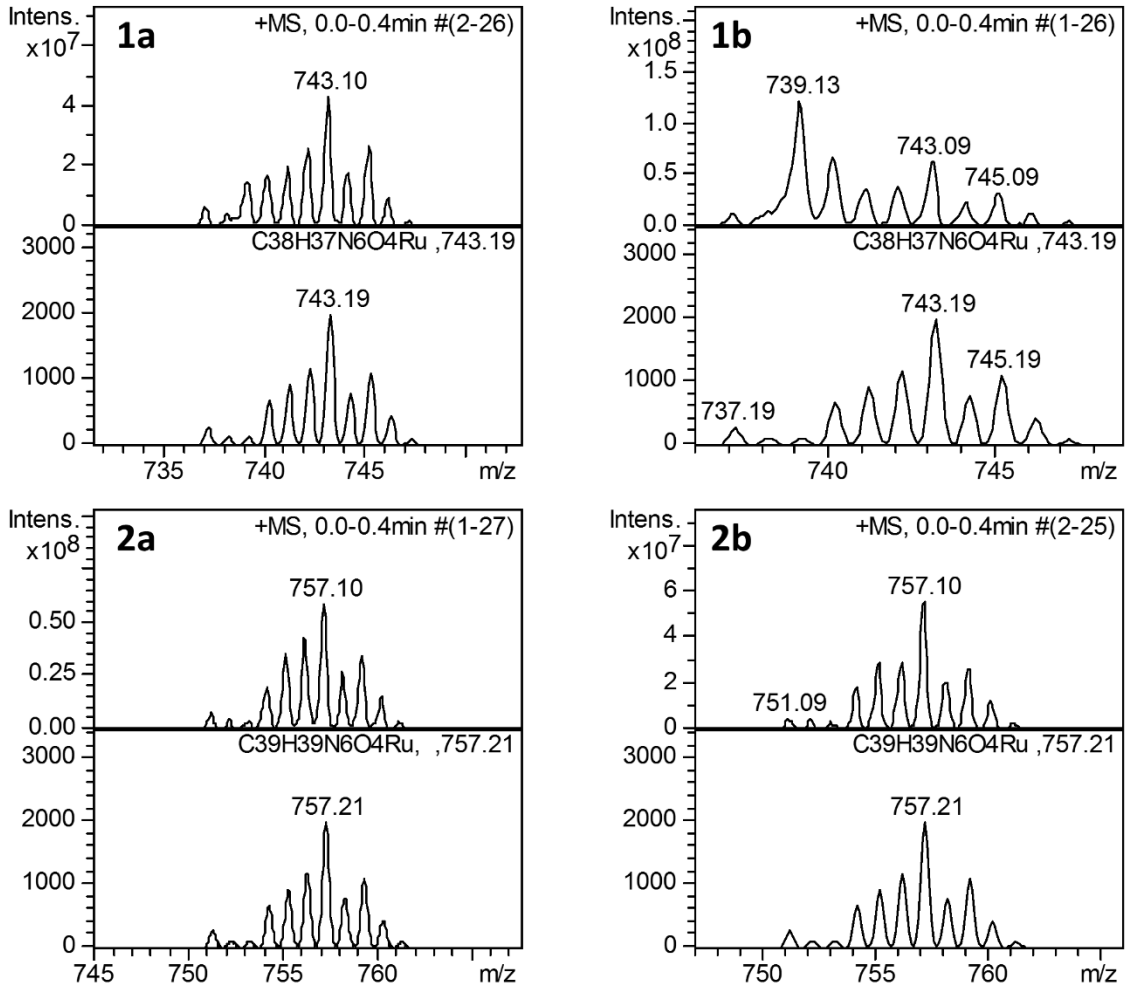

Figure S16. Experimental (top) and simulated (bottom) mass peak distribution corresponding to the adducts of 9-ethylguanine with the ruthenium complexes **1a-b** and **2a-b** showed in Figure S15.

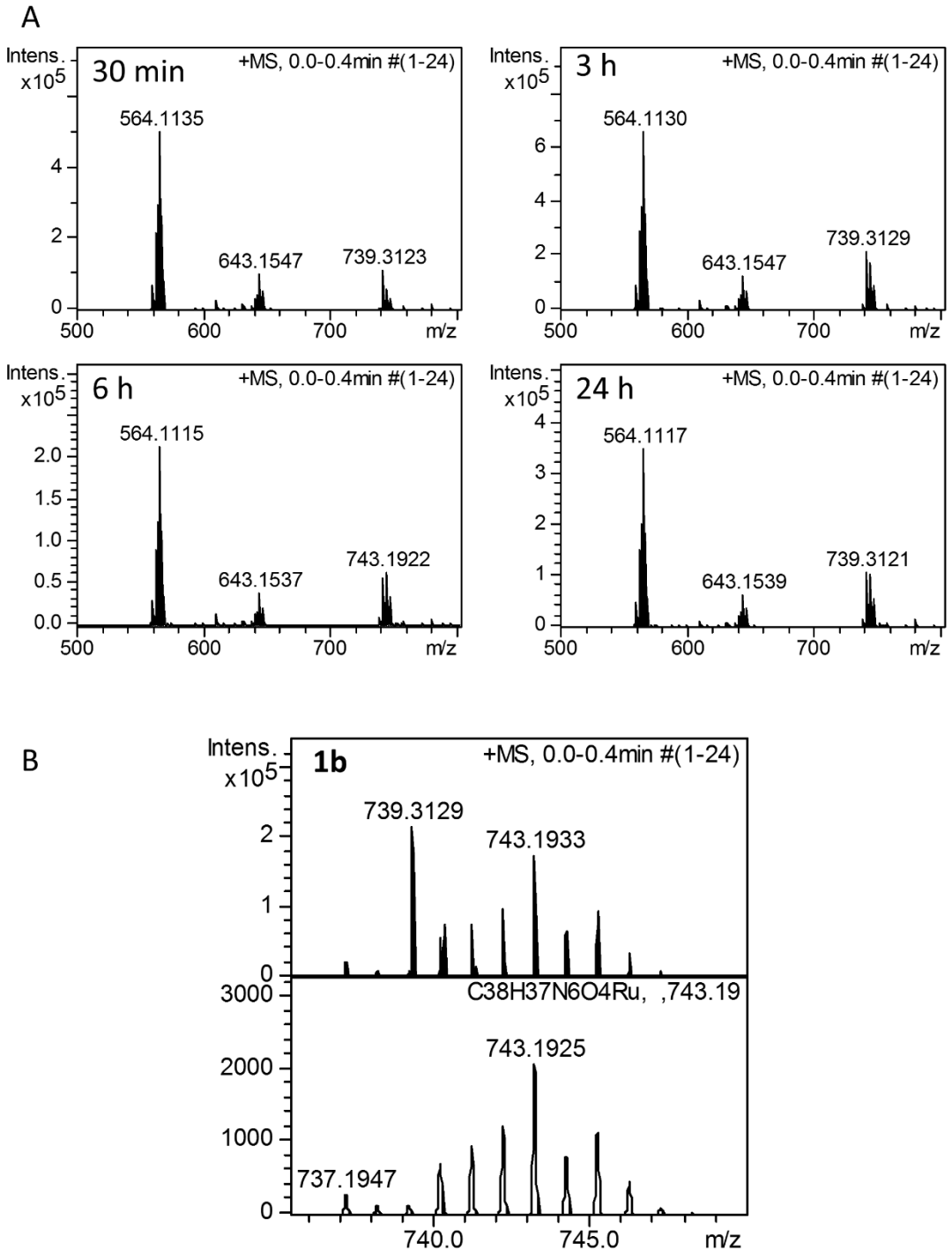

Figure S17. A) Time-dependent high-resolution mass spectra of 9-ethylguanine incubated with the ruthenium complex **1b**. No changes are observable between the 30 min and 24h time points, indicating that the exchange between the pyridine and the nucleobase is fast. B) High resolution experimental and simulated mass peaks corresponding to the adduct of 9-ethylguanine with the ruthenium complexes **1b** upon the loss of the pyridine ligand.

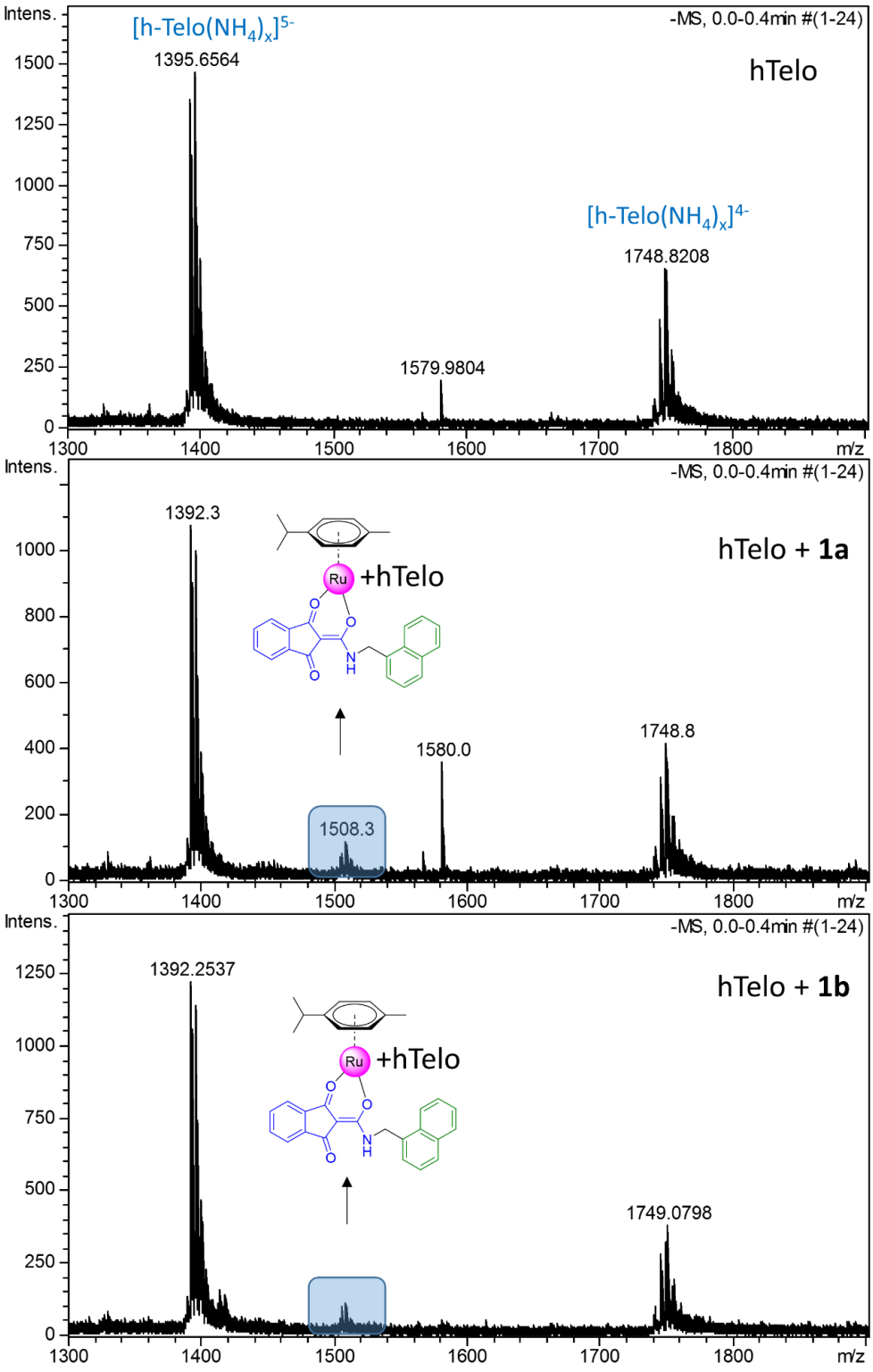

Figure S18. Mass spectra of prefolded *hTelo* G4 incubated (1 h) with the ruthenium complexes **1a** or **1b** (in a solution of ammonium acetate 50 mM). Final concentrations before injection were 10 µM for both G4 and the metal compounds. As indicated by the arrows, the peaks corresponding to the adducts formed by the G4 and the complex upon loss of chloride (**1a**) and pyridine (**1b**) are clearly visible.

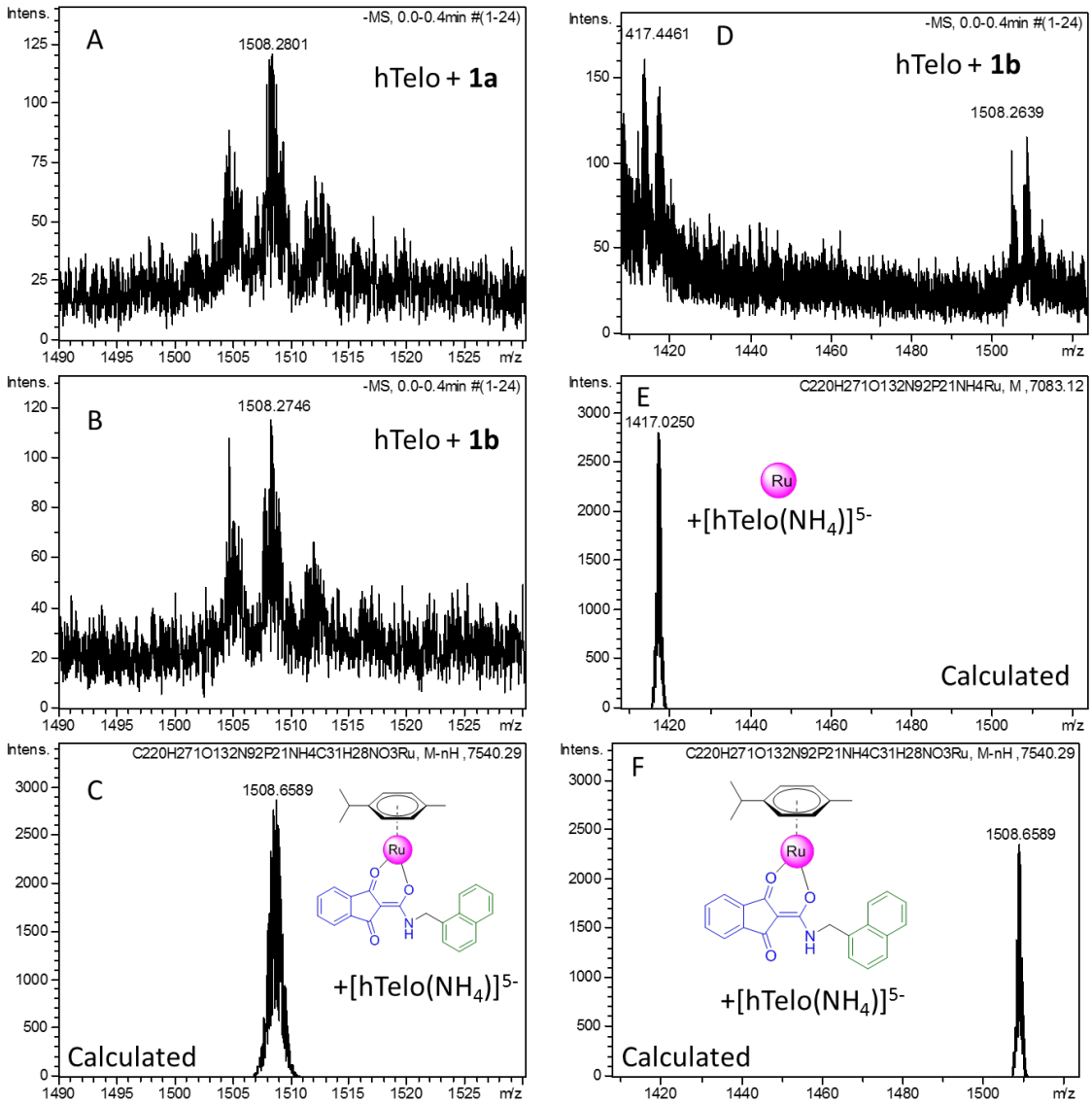

Figure S19. (Left column) Experimental mass peaks corresponding to the adducts of *h-Telo* with the ruthenium complexes **1a** (A) and **1b** (B) and simulated mass peak corresponding to the fregments reported in the picture (C). (Right column) Experimental mass peaks corresponding to the adducts of *h-Telo* with the ruthenium complexes **1b** (D) and simulated mass peak corresponding to the fragments reported in the picture (E and F).

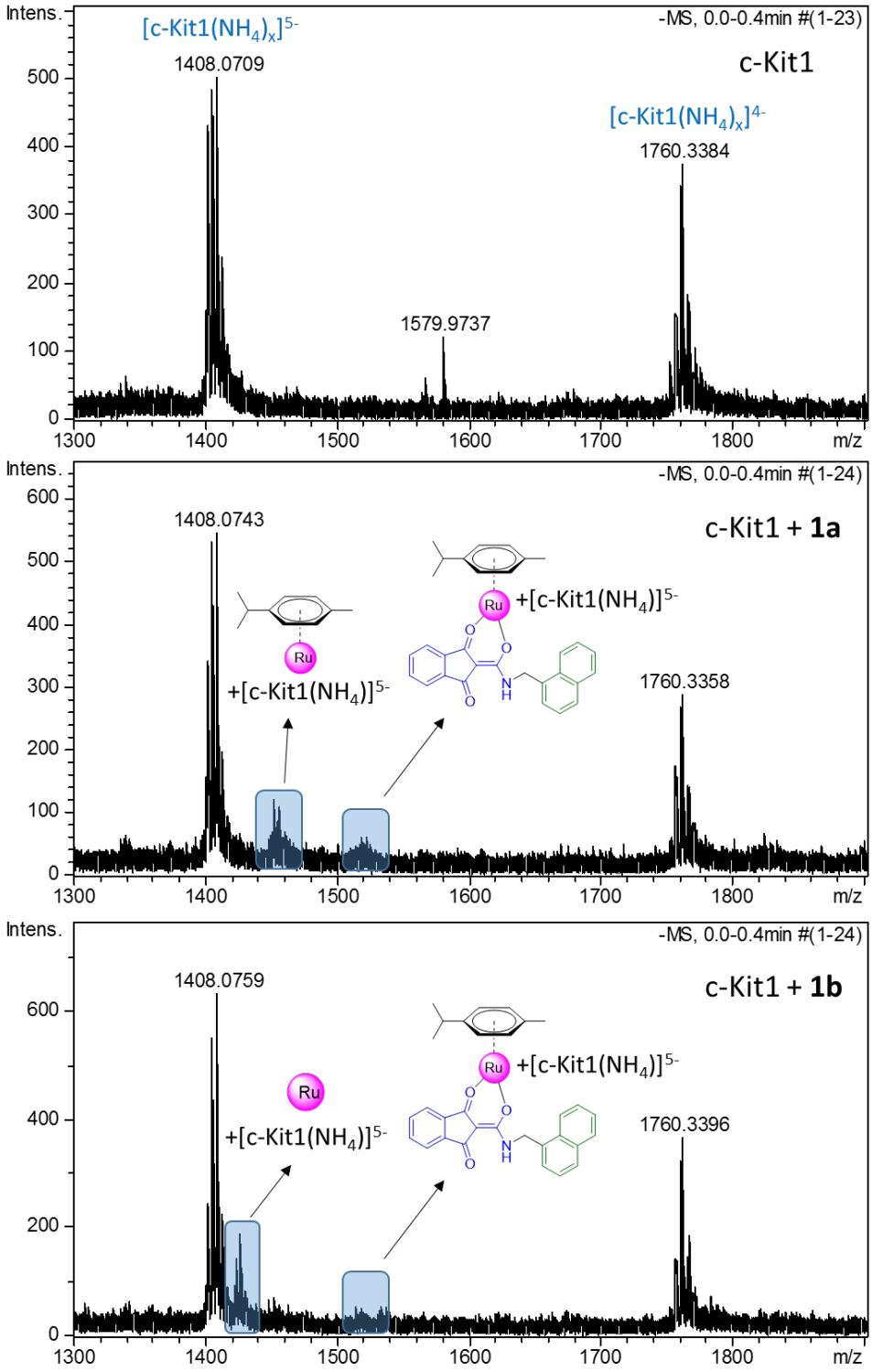

Figure S20. Mass spectra of prefolded *c-Kit1* G4 incubated (1 h) with **1a** or **1b** (in a solution of ammonium acetate 50 mM). Final concentrations before injection were 10 μM for both G4 and the metal compounds. As indicated by the arrows, the peaks corresponding to the adducts formed by the G4 and the complex upon loss of chloride (**1a**) and pyridine (**1b**) are visible, even if of low intensity. Furthermore, other fragmentation peaks are observable: one peak corresponds to the adduct formed by the G4 and the metal complex upon loss of both the chloride and the chelating ligands (see *c-Kit1*+**1a** spectrum), the other peak correspond to the fragment formed by the G4 and the Ru center upon loss of every ligand (see *c-Kit1*+**1b** spectrum).

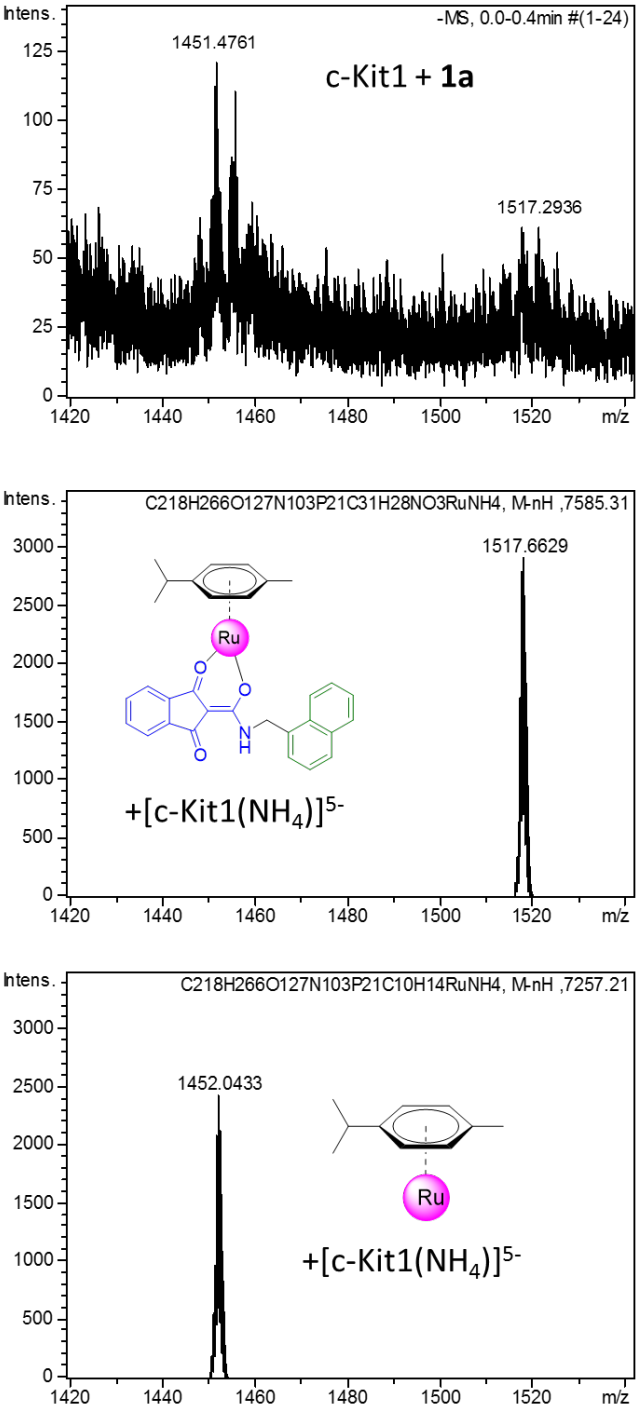

Figure S21. Experimental and simulated mass peaks corresponding to the adducts of *c-Kit1* with the fragments of ruthenium complex **1a** represented in the corresponding pictures.

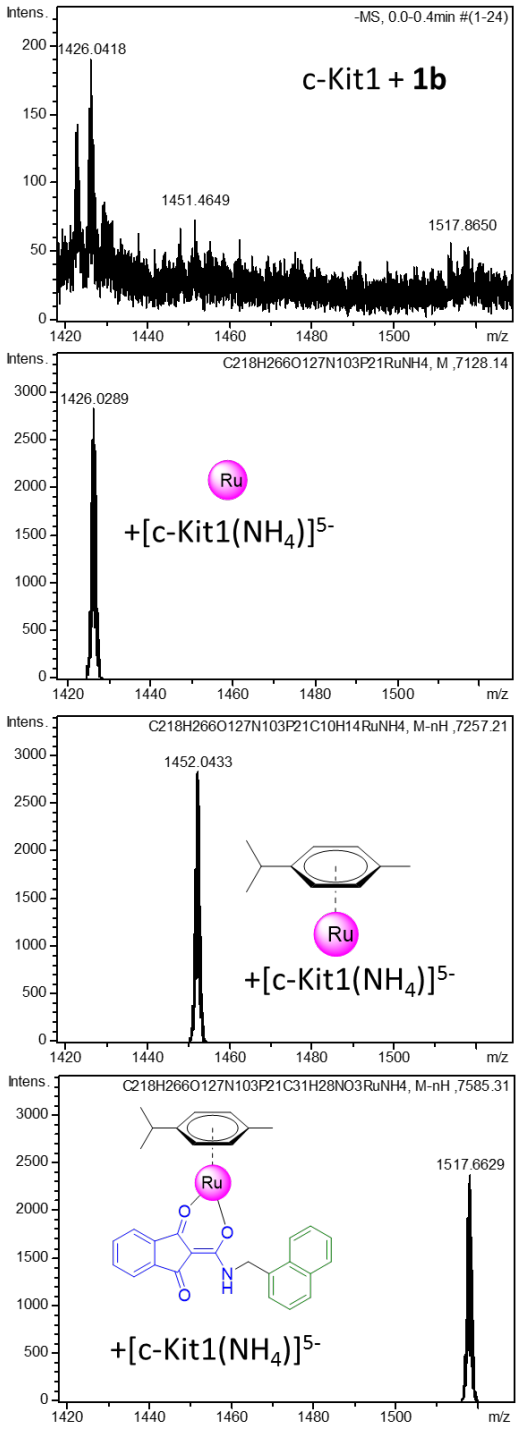

Figure S22. Experimental and simulated mass peaks corresponding to the adducts of *c-Kit1* with the fragments of ruthenium complex **1b** represented in the pictures.

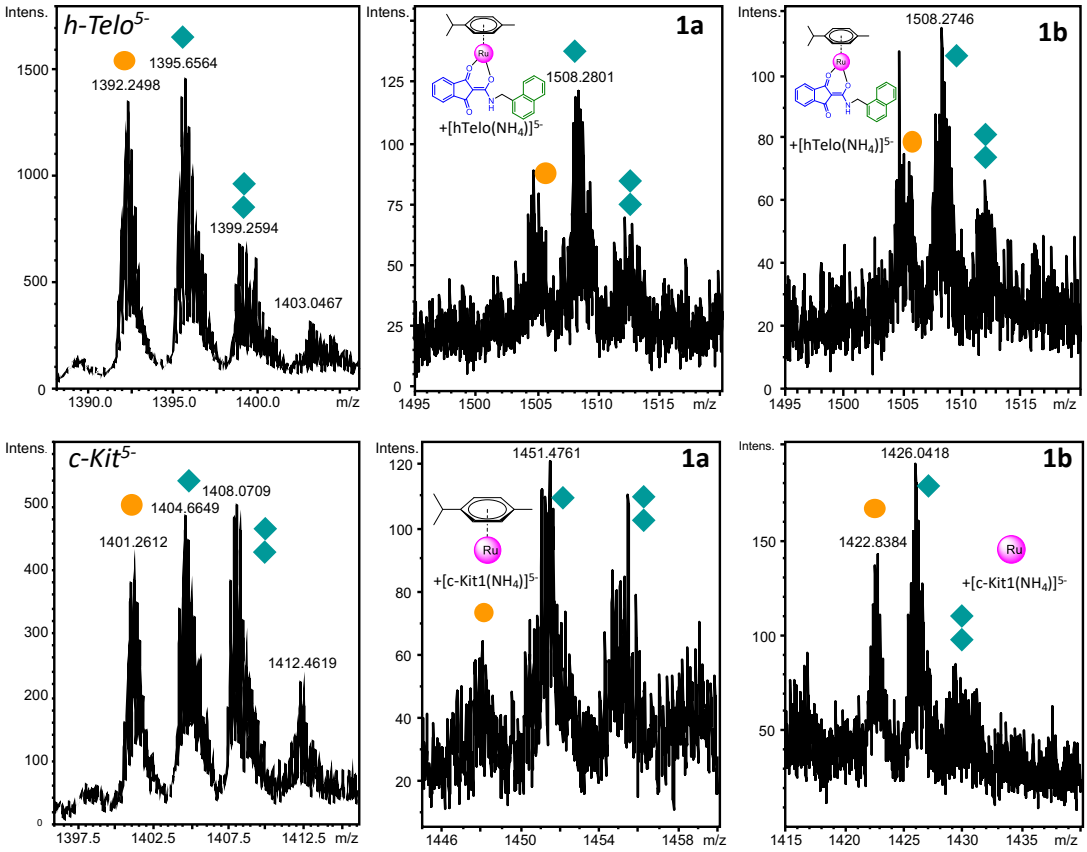

Figure S23. Negative ESI-TOF-MS enlargements of the distribution of ammonium adducts for the 5- charge state of 10 μM *hTelo* (top) and (bottom) *c-Kit1* sequences and of the corresponding G4-**1a/1b** adducts. The three peaks in each spectrum correspond to the ammonium free oligodeoxynucleotide (orange circles), one NH_4^+ ion adduct, and two NH_4^+ ions adduct (one and two green diamonds, respectively). In the case of *hTelo*, the peaks corresponding to the species formed by the G4 and the complex upon loss of chloride (**1a**) and pyridine (**1b**) were selected for comparison with the free G4. In the case of *c-Kit1*, the peaks corresponding to the species formed by the G4 and the complex upon loss of chloride and the chelating ligand (**1a**) and all ligands (**1b**) were selected for comparison with the free G4. For both *h-Telo* and *c-Kit1*, a decrease of the peak corresponding to the ammonium free oligodeoxynucleotide was observed, indicating a stabilization effect.

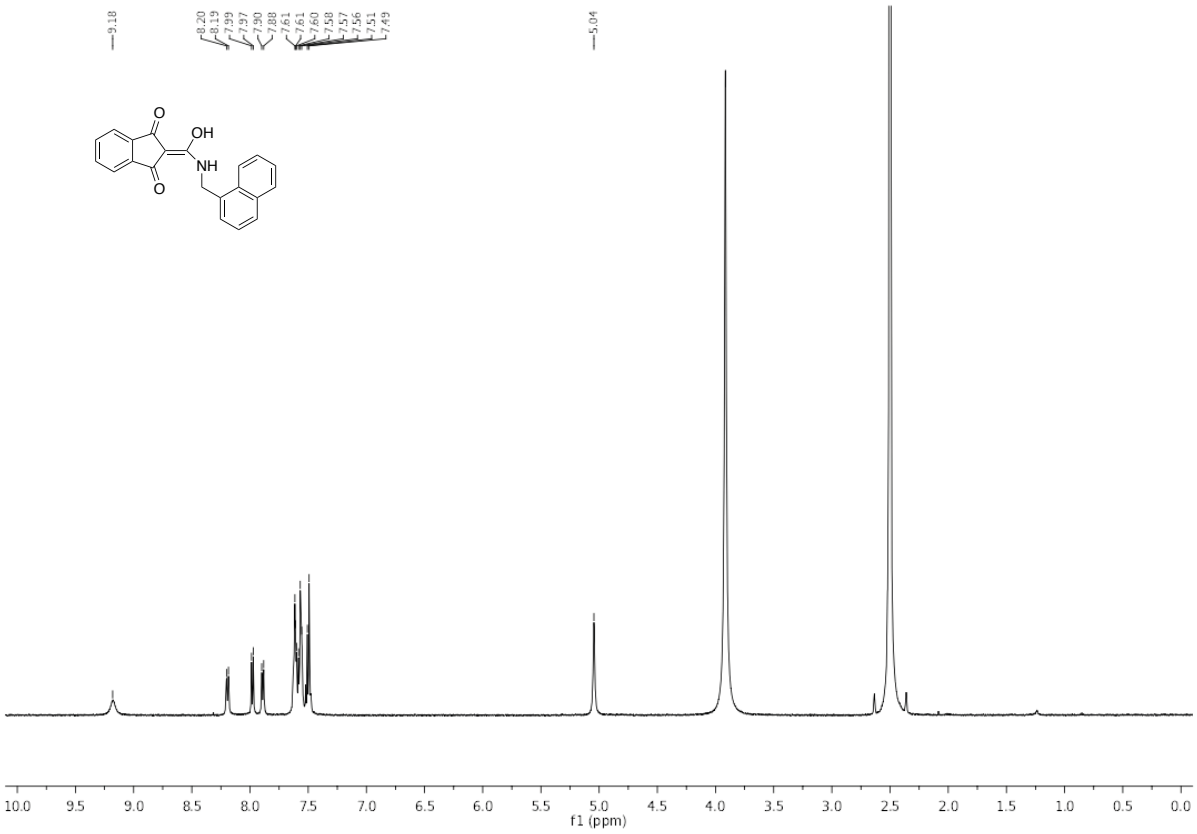

Figure S24. ^{1}H-NMR spectrum of **L1** in deuterated DMSO.

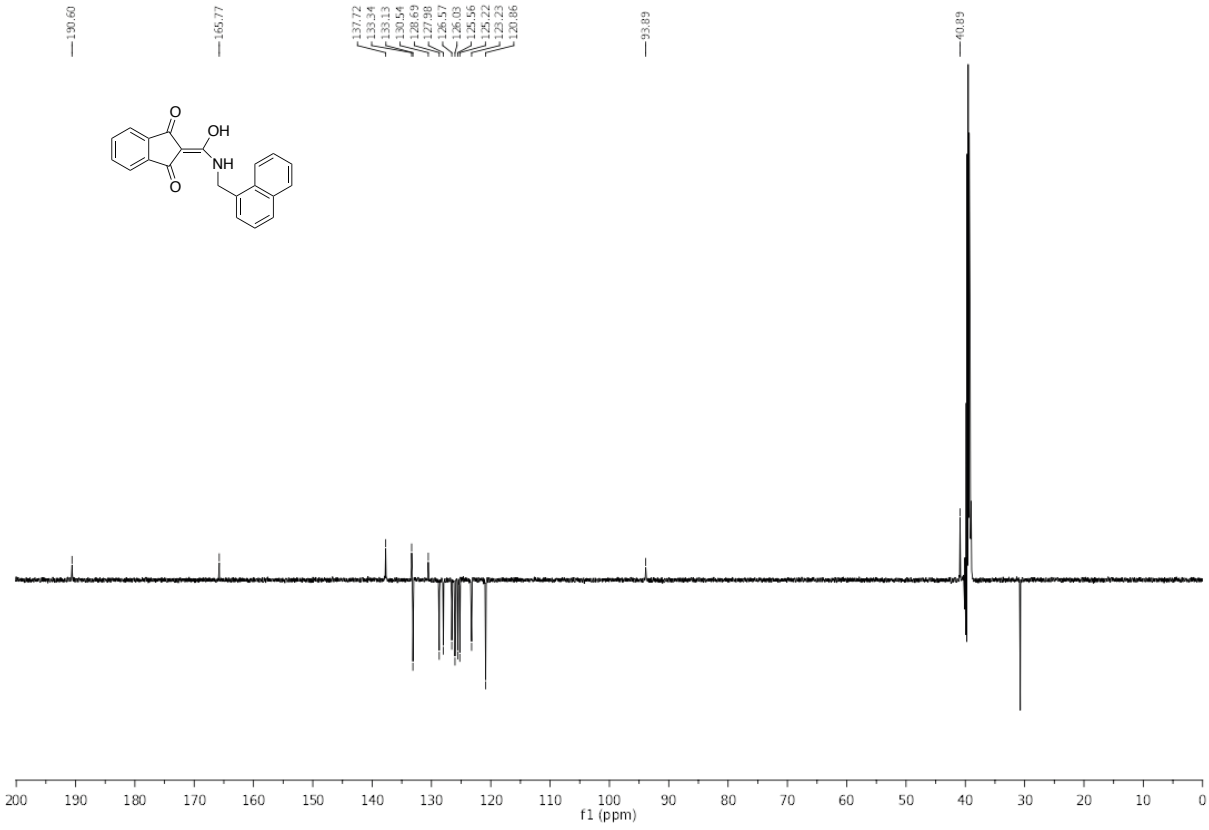

Figure S25. ^{13}C-NMR spectrum of **L1** in deuterated DMSO.

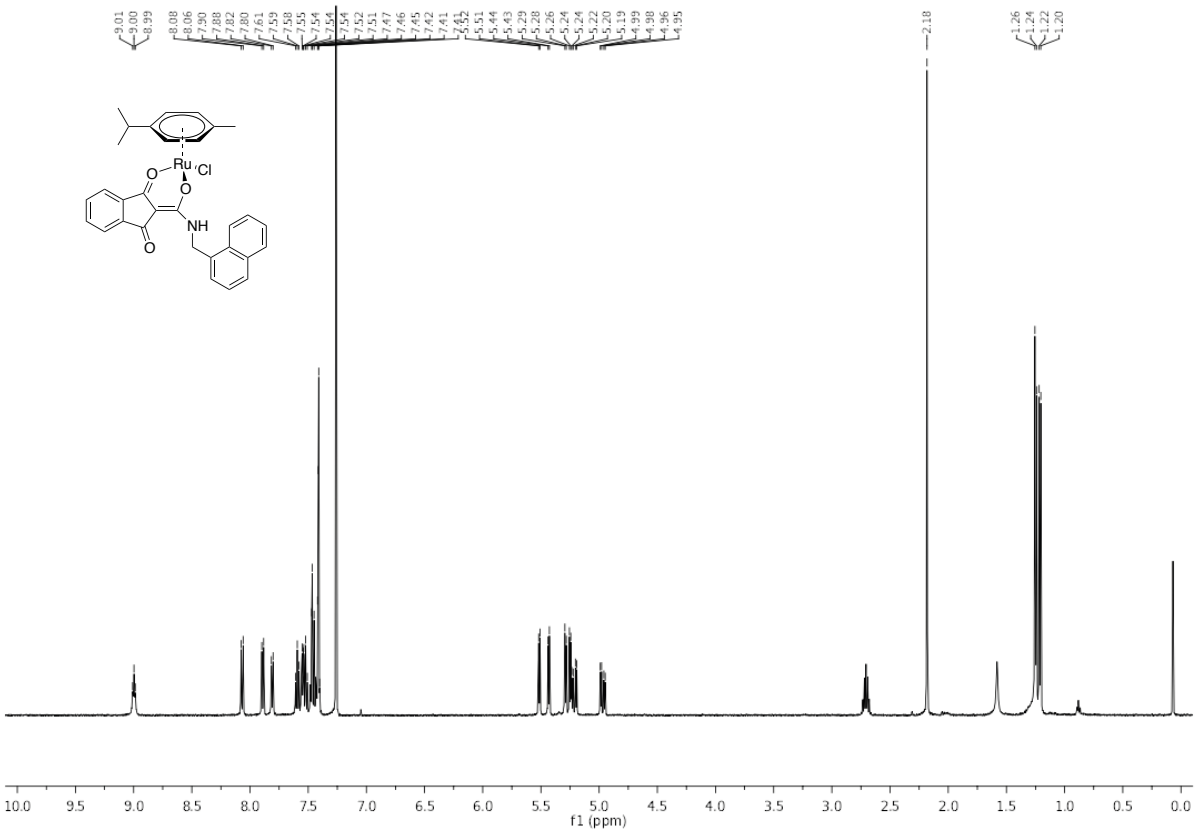

Figure S26. ^{1}H-NMR spectrum of **1a** in $CDCl_3$.

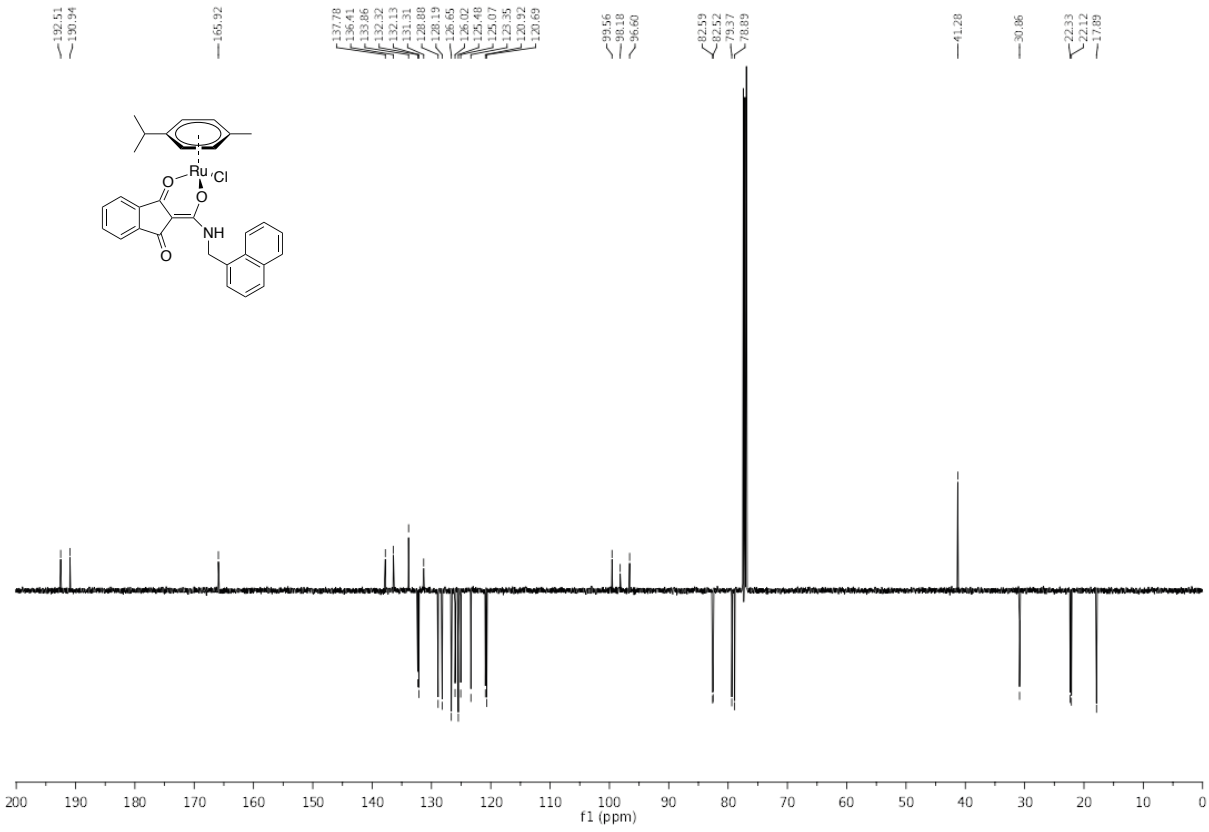

Figure S27. ^{13}C-NMR spectrum of **1a** in $CDCl_3$.

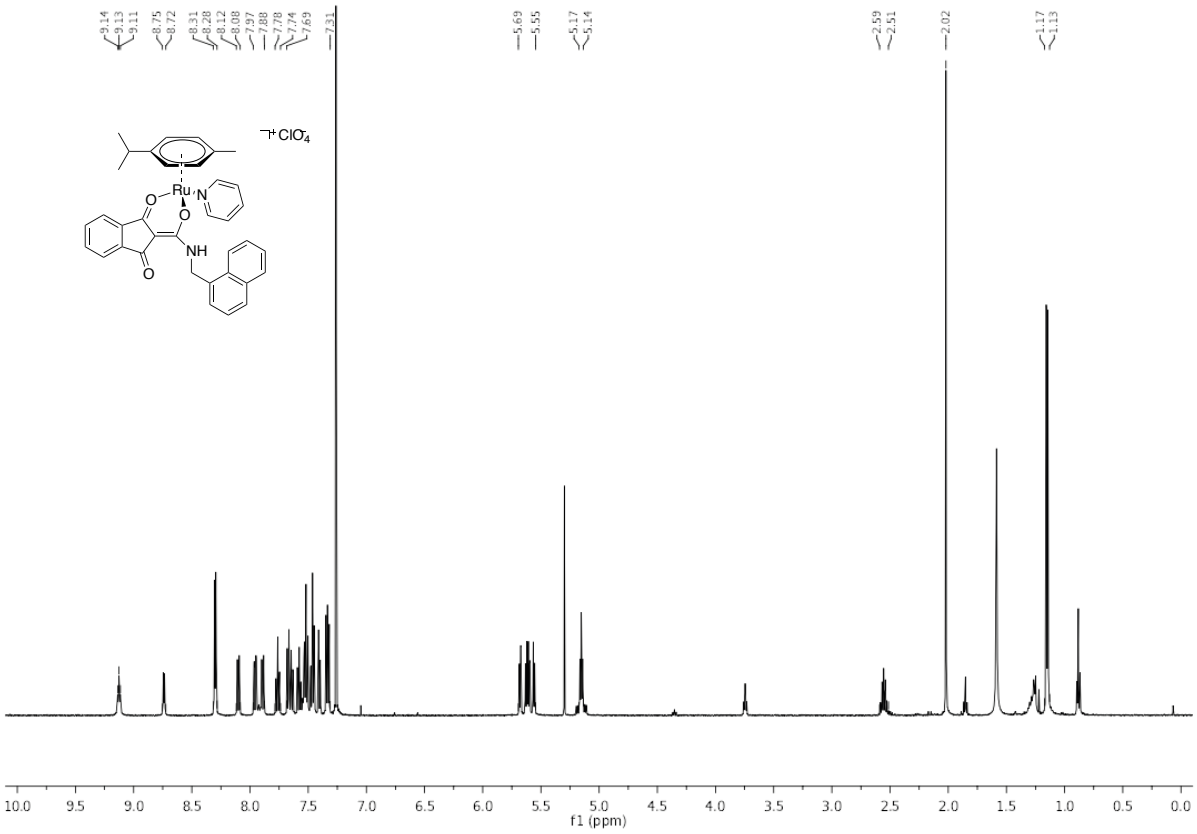

Figure S28. ^{1}H-NMR spectrum of **1b** in $CDCl_3$.

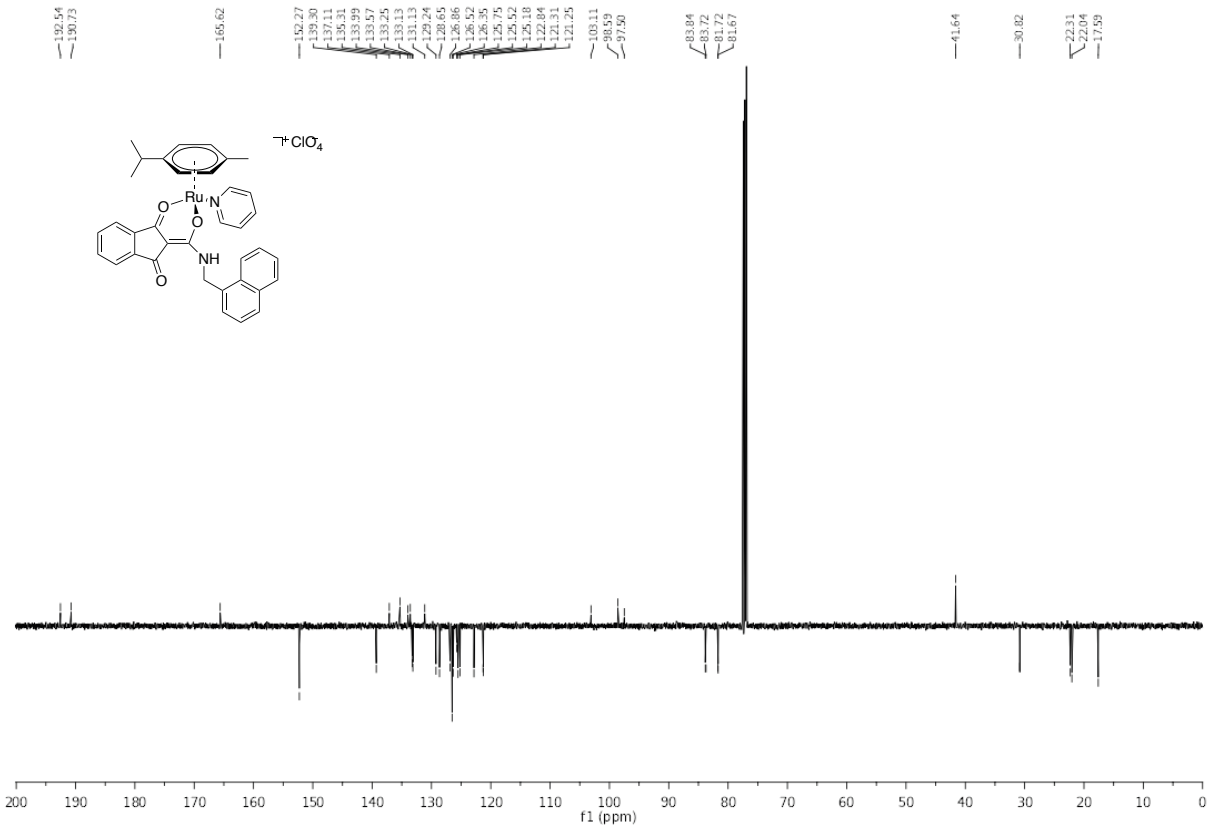

Figure S29. ^{13}C-NMR spectrum of **1b** in $CDCl_3$.

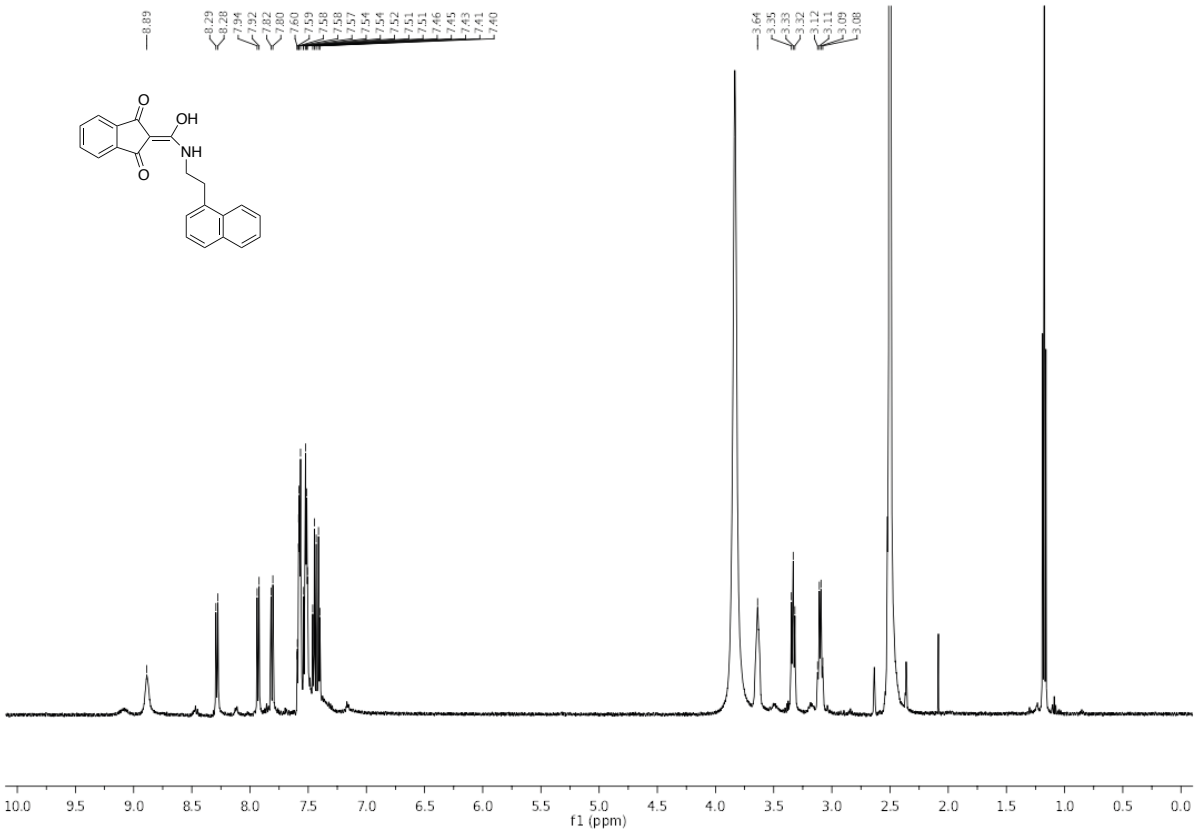

Figure S30. ^{1}H-NMR spectrum of **L2** in deuterated DMSO.

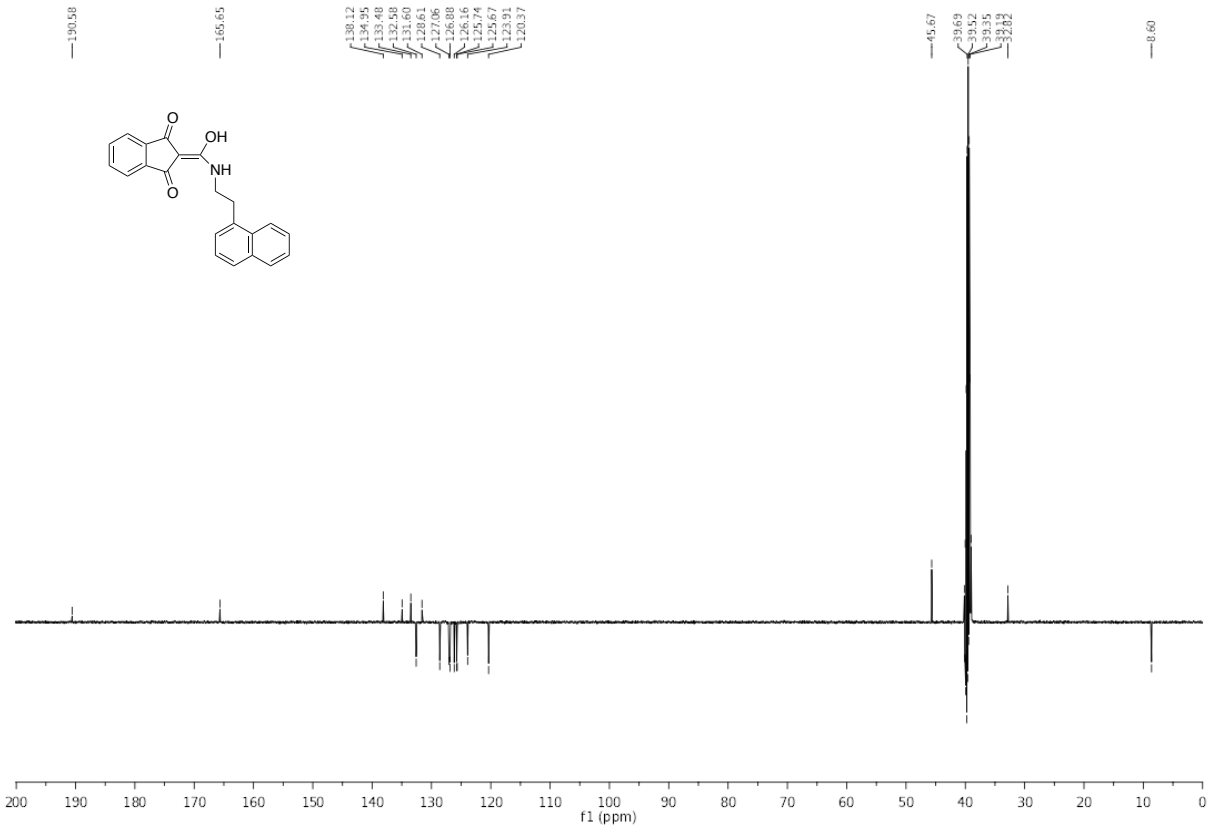

Figure S31. ^{13}C-NMR spectrum of **L2** in deuterated DMSO.

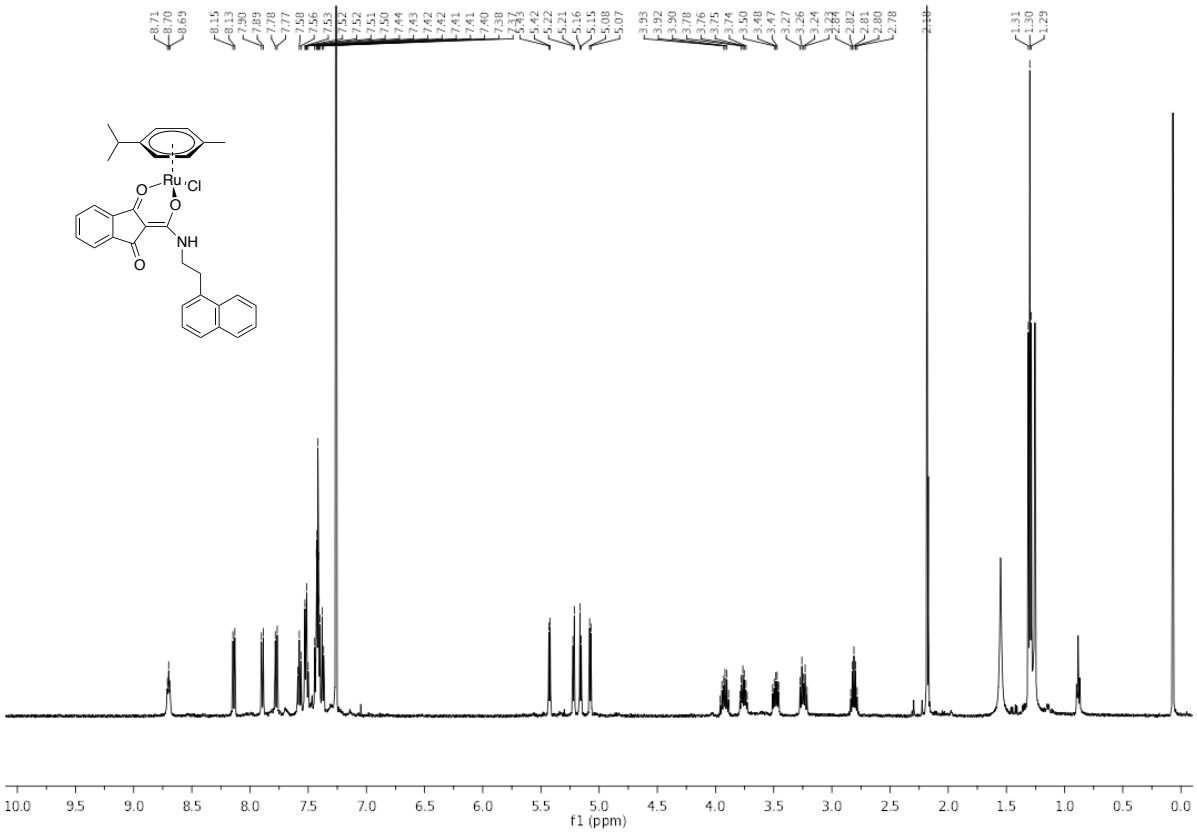

Figure S32. ^{1}H-NMR spectrum of **2a** in $CDCl_3$.

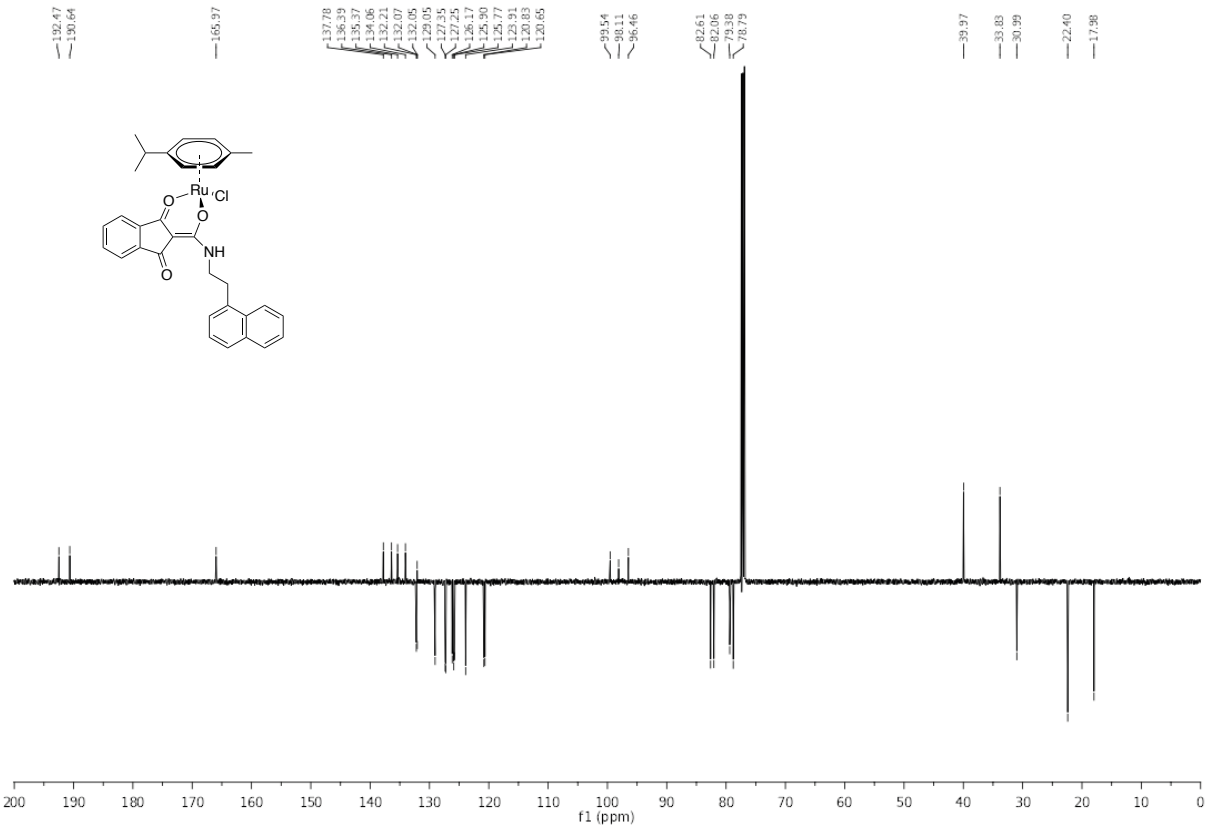

Figure S33. ^{13}C-NMR spectrum of **2a** in $CDCl_3$.

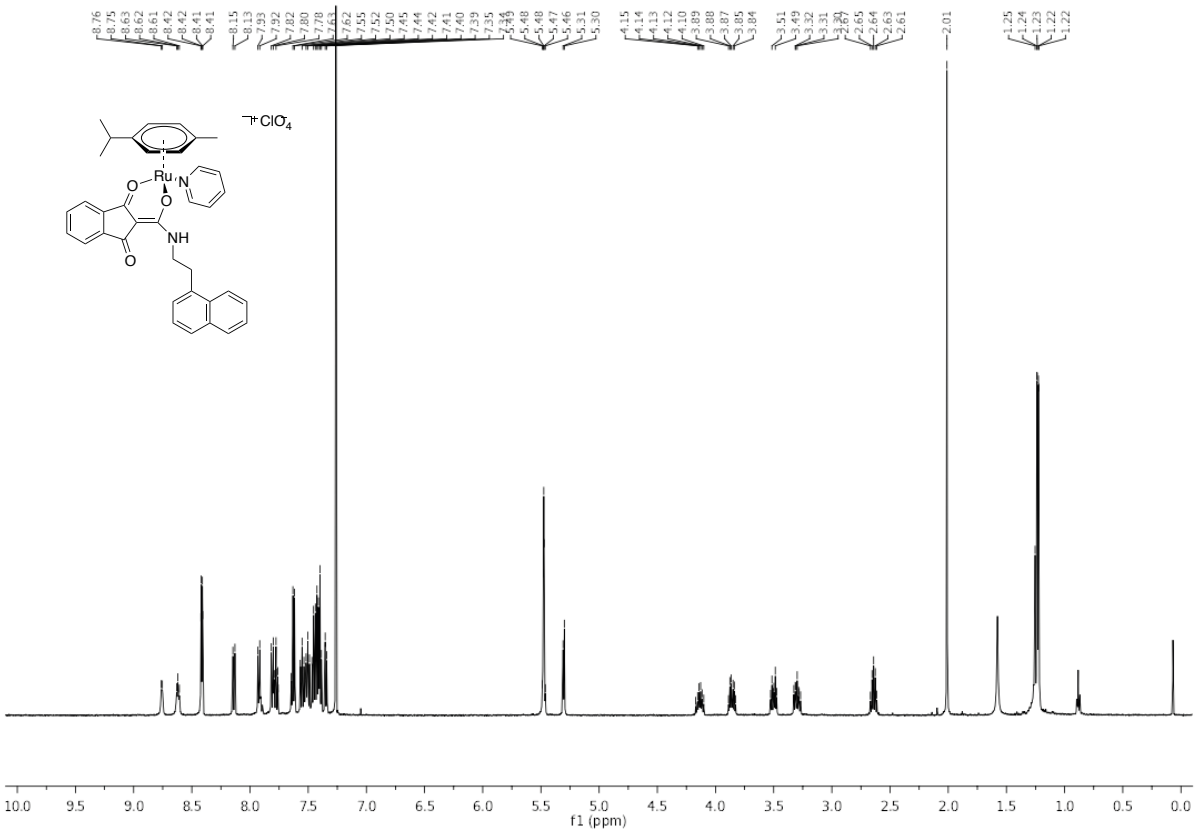

Figure S34. ^{1}H-NMR spectrum of **2b** in $CDCl_3$.

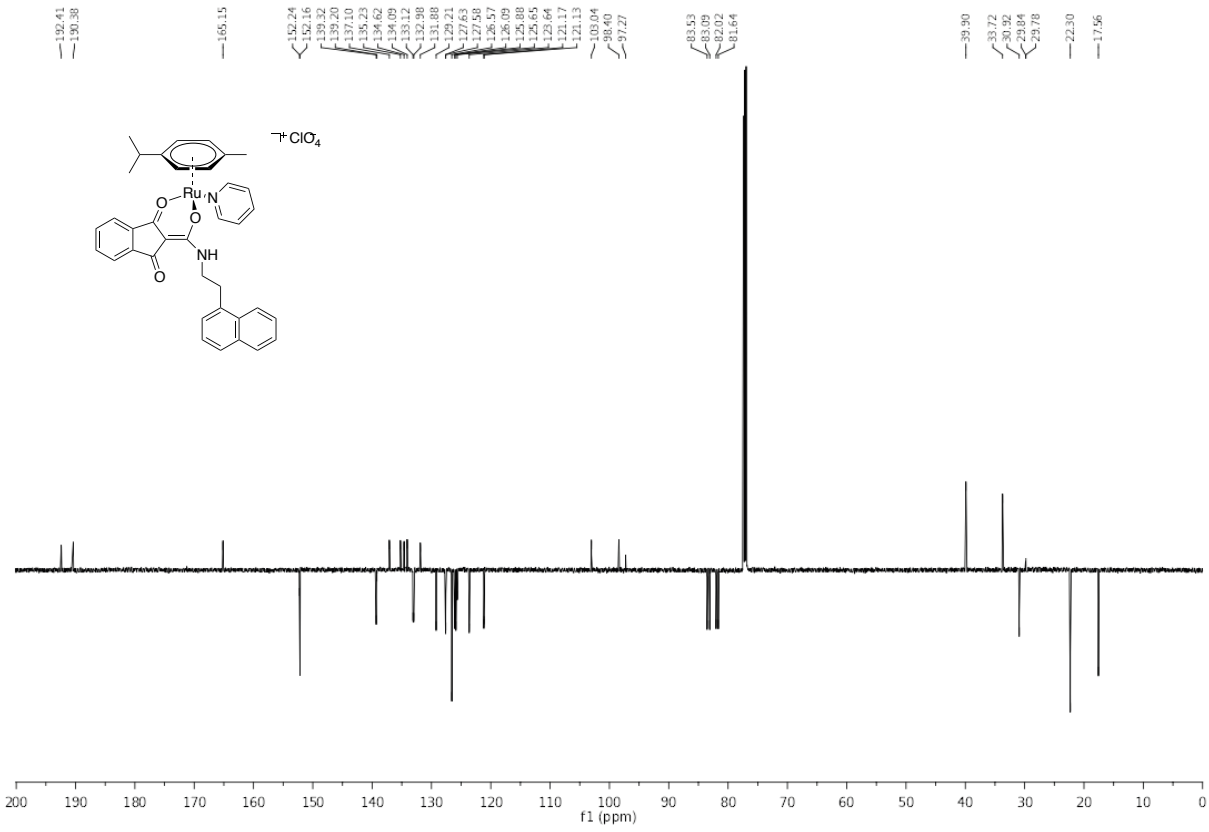

Figure S35. ^{13}C-NMR spectrum of **2b** in $CDCl_3$.